

We thank the reviewers for the thorough comments and suggestions to improve the manuscript. Below we reply to the reviewer's comments point by point. We list the comments in black, [our replies in blue](#), [original text for change in red](#) and [revised text in green](#).

Anonymous Referee #1

General comments

The manuscript of Y. M. Qin et al. presents the characteristics of fine PM in Hong Kong (chemical composition, size distribution, degrees of oxygenation, photochemical production and organic mass spectra) based on high resolution time-of-flight aerosol mass spectrometer (HR-ToF-AMS) measurements, positive matrix factorization (PMF) and air mass back-trajectory analyses. The manuscript is well structured and presented in a clear way. The methods used (PMF, back-trajectory analysis) are not innovative but are valid and well applied. The conclusions of this manuscript (e.g. the influence of meteorological conditions, particle mixing state, and the importance of photochemical aging on SOA formation in areas with high PM concentrations) are of scientific significance. I therefore recommend publishing this work in Atmospheric Chemistry and Physics after the authors respond to the following comments.

Specific comments

1. Page 3, Line 47-49: it should be more careful for the statement that SVOOA is a proxy for fresh SOA while LVOOA is aged SOA. There isn't an absolute relationship between the "fresh" / the "aged" (terms involved in the OA formation and evolution) and the volatility / oxidation state (terms for OA physicochemical properties). The description in Page 8744 of Li et al. (2013) could be considered to be adopted in this study: "less-oxidized OA (e.g. SVOOA)" and "more-oxidized OA (e.g. LVOOA)". Other statements about "fresh" SOA (SVOOA) and "aged" SOA (LVOOA) in other parts of the text (e.g. abstract) are suggested to be adjusted.

[Agree. Changes have been made as suggested. We adopt descriptions in Li et al. \(2013\).](#)

2. Page 9, Line 192-193: "aged" is an ambiguous term and the ageing process includes several specific mechanisms. I suggest that "aged" is replaced by more specific descriptions. In addition, as you stated that small particle proportions are higher in both LWC and IR episodes, are the underlying

reasons/mechanisms the same for both LWC and IR episodes? More specific discussion is suggested to replace “stronger local influences”.

We agree that “aged” is an ambiguous term. We aim at distinguishing “aged” vs. fresh. However, it is hard to distinguish the underlying mechanisms of ageing based on the type-averaged size distributions of organics and sulfate mass only. Although the fractions of small particles are higher in both LWC and IR episodes than in LRT episodes, the underlying mechanisms may be different. We have discussed the possible mechanisms combining with the other observational results (e.g. diurnal variations, elemental analysis of OA, mixing state and size variations before and during these episodes) in the original manuscript. We have clarified it in the revised manuscript as below.

Change from:

Within each type of episode, sulfate had a smaller portion of small particle mode than organics did, indicating that sulfate was mostly aged while local activities resulted in some fresh emissions of organics. LWC episodes had the largest small mode contribution and LRT episodes had the smallest, providing additional support that particles were more aged and large particles dominated in LRT episodes while the proportion of fresher small particles was higher in LWC and IR episodes due to stronger local influences.

To:

Within each type of episode, sulfate had a smaller fraction of small particle mode than organics did, indicating that sulfate was relatively aged while organics received contributions from local fresh emissions. LWC episodes received the largest contribution from small mode sulfate because of some local influences whereas LRT episodes received the smallest contribution with relatively little local activities. The oxidation mechanisms, however, might be different. Aqueous phase oxidation may dominate in LWC episodes while photochemical oxidation may dominate in IR episodes.

3. Page 9, Line 194-197: The accuracy of the derived particle mixing state from AMS is suggested to be discussed with comparing with single-particle instruments. Line 211: comparison with previous studies about the mixing state in Hong Kong will be helpful.

Thanks for the insightful suggestion. It would be very useful to compare the data of the AMS with single-particle measurements. However, we did not have a single particle spectrometer at our disposal in this campaign. We admitted that this is one of the limitations of the current study.

In this study, we infer the mixing state of the components based on overlapping of their size distributions, similar to Bahreini et al.(2003). It is understood that overlapping of size distributions is a necessary but not sufficient condition for internal mixing. Hence, our discussion of the mixing states is qualitative but not quantitative. To our best knowledge, direct measurements of mixing state from single particle instruments across different seasons in Hong Kong have not been reported. Based on the AMS size distributions, we found that sulfate and organics in large particles were mixed internally only in LWC episodes, and were more likely to be externally mixed in IR and LRT episodes. Freshly formed small particles are externally mixed in all types of episodes. We hope that this study may add to a better understanding of organic and sulfate mixing states in Hong Kong. We have added the above discussions in the revised manuscript.

4. Page 10, Line 213-217: How those percentage numbers are calculated for the size variations? Line 219-220: How do you derive this result that “Since the particles were fresher and smaller during the days before episodes, they grew more rapidly as gas phase semi-volatile components condensed on the particles”? Is condensation the only contributor to the particle growth? Line 220-221: Please show evidence to support “the number concentrations of the pre-existing particles were lower before than during the episodes”. Why the size variations for the LRT episodes are overlooked? What is your object to show the sizes variations? What are the implications?

The calculation of size variation and the number concentration have been clarified in the revised supplementary information. We did not focus on the size variations of the LRT episodes because it is difficult to assess what has happened to the particles before they reached the site based on measurements at the site. The particles were already aged when they reached the site. With little local aging, the size variation analysis may not give us further information on the characteristics of ageing. Instead, we would like to focus on LWC and IR episodes which have shown signs of local atmospheric processing.

Change from:

Figure 6 shows that, in the two LWC episodes, the size variations for both the small and large modes

were less obvious: -2.5% for organics small mode, +8.1% for organics large mode, +1.6% for sulfate small mode, and -3% for sulfate large mode from start to end as shown in the figure. By contrast, the size variations in the IR episodes were much more drastic: +51.3% for organics small mode, +40.5% for organics large mode, +45.4% for sulfate small mode, and +35.9% for sulfate large mode. Furthermore, particle sizes usually increased more rapidly during the days before the IR episodes (days shaded in blue in Figure 6) than during the actual episodes (days shaded in orange). Since the particles were fresher and smaller during the days before episodes, they grew more rapidly as gas phase semi-volatile components condensed onto the particles. Moreover, the number concentrations of the pre-existing particles (acting as condensation nuclei) were lower before than during the episodes, rendering more rapid size increases before the episodes.

To:

As discussed earlier, there may be some local atmospheric processing of aerosols in LWC and IR episodes but not in LRT episodes. Therefore, we further explored the mechanisms underlying the atmospheric processing of LWC and IR episodes based on the size variations before and during episodic events. Figure 6 shows the particle mass mode diameters and areas (concentrations) in the LWC and IR types of episodes. We obtained the percentage changes in mode diameters by comparing the smallest diameter before the episode and the largest diameter during the episode for each episode. These percentages in each episode was then averaged to obtain the percentage changes for each episode type. The results show that the changes in mode diameter were small in the LWC episodes: -2.5% for small mode organics, +8.1% for large mode organics, +1.6% for small mode sulfate, and -3% for large mode sulfate. In contrast, the changes in mode diameters changes were much more drastic in the IR episodes: +51.3% for small mode organics, +40.5% for large mode organics, +45.4% for small mode sulfate, and +35.9% for large mode sulfate. Furthermore, particle size usually increased more rapidly before the IR episodes (shaded in blue in Figure 6) than during the episodes (shaded in orange). With fewer pre-existing particles before the episodes, particle growth likely via condensation and reactive uptake of semi-volatile components was more rapid than during the episodes. The number concentration is discussed in detail in SI.

SI:

Figure S7 shows the variations in the 24-h average of the fitted mode diameters and peak areas (and

indicator of mass concentration in that mode) of sulfate and organics during IR episodes. All mode diameters and the peak areas increased from before the episode (the blue shaded area) to during the episode (the orange shaded area). The extent of the peak area increase (mass concentration increase) exceeds what can be explained by the increase in mode diameter alone assuming spherical particles and constant number concentrations. As shown in Table S1, the increases in peak areas are always larger than the increase in the cube of mode diameters for both modes. This suggests an increase in the number concentration of particles during the episodes. The lower number concentrations of pre-existing particles before the episodes renders more rapid increases in size than during the episodes.

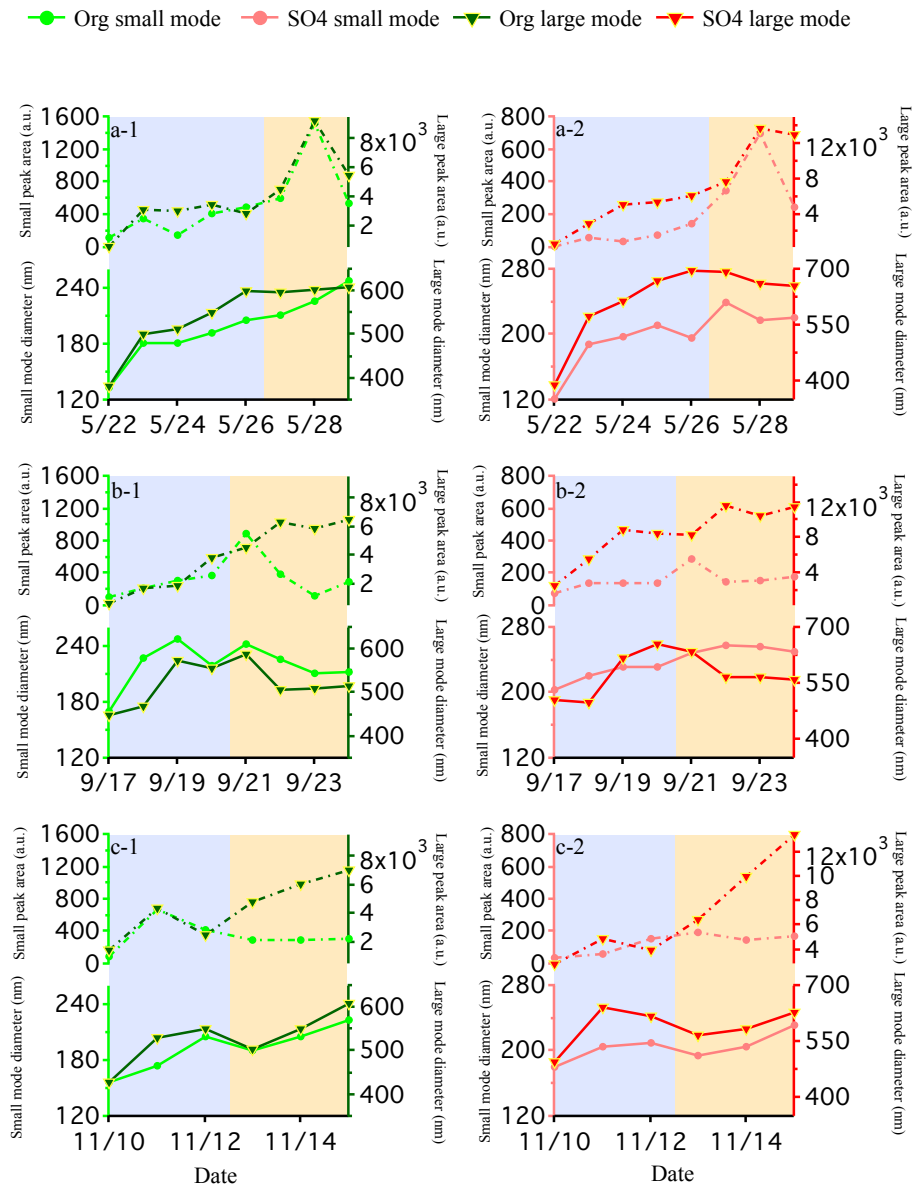


Figure S1' Variations of 24-h averaged of the fitted mode diameters and peak areas of organics (1) and sulfates (2) before (shaded blue) and during (shaded orange) each IR episode.

Table S1. Mode diameters and peak areas before and during episodic days in each of the three IR episodes.

		Before or During Episode	Small mode peak area (a.u.)	Large mode peak area (a.u.)	Small mode diameter (nm)	Large mode diameter (nm)	Peak area ratio During : Before	Ratios of cube of mode diameter During : Before
IR-1	Org	Before	312	2621	178	509	2.84 (small mode)	2.10 (small mode)
		During	886	6415	228	603	2.45 (large mode)	1.66 (large mode)
	SO4	Before	67	4051	183	589	6.44 (small mode)	1.88 (small mode)
		During	431	11421	226	671	2.82 (large mode)	1.47 (large mode)
IR-3	Org	Before	255	2051	216	513	1.69 (small mode)	1.09 (small mode)
		During	430	5808	223	531	2.83 (large mode)	1.11 (large mode)
	SO4	Before	127	6358	222	570	1.54 (small mode)	1.49 (small mode)
		During	195	10513	254	582	1.65 (large mode)	1.06 (large mode)
IR-5	Org	Before	165	2778	179	503	1.85 (small mode)	1.54 (small mode)
		During	305	5983	207	555	2.15 (large mode)	1.34 (large mode)
	SO4	Before	86	3880	198	585	1.97 (small mode)	1.20 (small mode)
		During	170	9980	211	593	2.57 (large mode)	1.04 (large mode)

5. Page 10, Section 3.4 could be merged into Section 3.1 or just after the Section 3.1 (moving Section 3.2 to 3.3. . .).

Changed as suggested.

6. Page 12, Line 275: Please replace Figure 9c by Figure 9a.

Changed as suggested.

Anonymous Referee #2

General comments

The authors showed scientific findings on role of photochemistry in the evolution of secondary PM characteristics base on analyses of measurement data with high temporal resolution. The manuscript is generally well written and constructed, and therefore may be suitable for future publication in Atmospheric Chemistry and Physics after revisions based on referees' and other relevant comments. In addition, I recommend the authors to highlight the remarkable progress from their previous studies because they have already published several papers on the measurement data used in this study.

We have highlighted some key findings from our previous studies and the unique aspects of this study in the introduction.

Change from:

We conducted four one-month campaigns in each of the four seasons at the Hong Kong University of Science and Technology (HKUST) Air Quality Research Supersite (AQRS) from May 2011 to February 2012 using an Aerodyne HR-ToF-AMS for non-refractory PM₁ (PM with aerodynamic diameter less than 1 micron). We have previously examined the general characteristics (Lee et al., 2013; Li et al., 2013, 2015), seasonal trends (Li et al., 2015), aqueous-phase process in the formation of oxygenated organics (Lee et al., 2013; Li et al., 2013, 2015), organic sulfur compounds (Huang et al., 2015), and particle hygroscopicity (Meng et al., 2014; Yeung et al., 2014). Most of these studies did not explore in detail the evolution of PM characteristics on the timescale of hours. The current work thus focuses on high PM episodes lasting a day or several days across the seasons. Specifically, we aim to investigate the role of local photochemical activity in the formation and evolution of secondary aerosols based on the real-time chemical composition and size distribution data.

To:

We conducted four one-month campaigns in each of the four seasons at the Hong Kong University of Science and Technology (HKUST) Air Quality Research Supersite (AQRS) from May 2011 to February 2012 using an Aerodyne HR-ToF-AMS for non-refractory PM₁ (PM with aerodynamic diameter less than 1 micron). In our previous studies, we found that photochemical oxidation during a haze episode

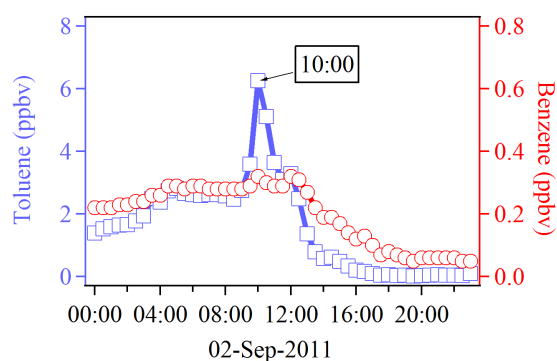
and aqueous-phase reactions during two foggy periods both led to a high degree of oxygenation of organics due to aging in gas phase and/or aqueous phase with substantial SOA formation (Lee et al., 2013 and Li et al., 2013). In spring and summer, SOA, with abundant SVOOA, was more likely to form locally. The oxygen-to-carbon atomic ratio (O:C) and average carbon oxidation state ($\overline{\text{OS}}_c$) peaked in the afternoon in spring and summer (Li et al., 2015). In autumn and winter, LVOOA dominated in SOA. The O:C ratio and $\overline{\text{OS}}_c$ showed little diurnal variation. Huang et al. (2015) estimated the contents of organic sulfur compounds in Hong Kong in September 2011. They highlighted the importance of both aqueous-phase processing and regional influence for the formation of organic sulfur compounds. Closure analysis was performed between the PM hygroscopicity measured by an hygroscopic tandem differential mobility analyzer (HTDMA) and chemical composition measured by an HR-ToF-AMS and a constant growth factor of 1.18 for organics was found to be adequate for a good closure, given the dominant contribution of the very hygroscopic sulfate at this suburban site (Cheung et al., 2016; Yeung et al., 2014). Meng et al. (2014) found that the aerosol hygroscopic parameter (k) decreased with an increasing organic-to-inorganic volume ratio. Furthermore, the concentration of cloud condensation nuclei (CCN) was found to be more sensitive to the mixing state and hygroscopicity of the particles at a high supersaturation (SS)=0.70% and a low SS=0.15%, respectively.

The above studies primarily focused on the analysis of campaign-average scenarios, without specifically looking at episodic events that occurred during the campaign. In the current study, we investigated the chemical transformation and size evolution of secondary aerosols in high particulate matter episodes across the four seasons. Specifically, we examined in detail the photochemical evolution in a particular episode in which local influences were dominant. Results from the current study reveal the rapid evolution of secondary aerosols and are relevant to other megacities with large precursor input and high photochemical activity.

Specific comments:

1. Page 6, Line 129-130: How can I find “no significant peaks of benzene and toluene after 10:00” from Fig. S3?

We have added the time series of benzene and toluene in supplemental information as shown below.



- Page 7, Line 147: Is the quite low fraction of POA even in cool season common in and around the study region, or specific at the study site (period)?

The HKUST supersite is located on the campus of HKUST, which sits on the hillside of Clear Water Bay on the east coast of Hong Kong that has relatively low population density. There is little local emission around the site. Two minor local sources include Clear Water Bay Road and a small student canteen. The Clear Water Bay Road is located outside of the campus and has mild traffic. The student canteen within 200m of the site, which operates only from 18:00LT (local time) until midnight. Therefore, it is not surprising that the POA fraction in our study is low even in cool season. As an indicator for primary PM, elemental carbon (EC) concentrations in PM_{2.5} via off-line analysis after filter sampling at this site from March 2011 to February 2012 were found to be low throughout the year ($0.86 \pm 0.53 \mu\text{g}/\text{m}^3$) (Huang et al., 2014). Such description has been added in the revised manuscript.

- Page 9. Line 197-199: If organics and sulfate are internally mixed, diameters of organics and sulfate are strongly correlated. However, is the strong correlation sufficient evidence for the internal mixing?

If the organics and sulfate are internally mixed (they exist in the same particle), their diameters should strongly correlate with each other and the growth rate of particle size should be similar (indicated by the slope of in Figure 5). The observed strong correlation and slope of unity (correlated in time and size) suggest that these species are likely internally mixed, although we cannot exclude out the possibility of external mixing. On the other hand, if the mode diameters of sulfate and organics did not change coherently with a strong correlation and a slope close to unity, these particles are more likely externally mixed. Using such correlations in size to indicate mixing states of species has been applied in previous field studies such as by Bahreini et al. (2003). It should be noted that these conditions of correlation and

slope are necessary but not sufficient evidence for internal mixing. In the original text, we stated that the large mode diameters of organics and sulfate (Pearson's R value equals to 0.7) were strongly correlated with a slope close to unity in LWC episodes (Figure 5), suggesting that organics and sulfate are likely internally mixed in large particles. We did not exclude the possibility of external mixing.

Pls also see our response to Comment #3 of Reviewer 1

Change from:

Various studies have analyzed the particle mixing state based on single-particle instruments such as the aerosol time-of-flight mass spectrometer (Healy et al., 2013, 2014; Yang et al., 2012) and the single-particle aerosol mass spectrometer (Wang et al., 2015). Particle mixing state can also be inferred from particle size information obtained with the AMS. The large mode diameters of organics and sulfate (Pearson's R value equals to 0.7) were strongly correlated with a slope close to unity in LWC episodes (Figure 5), suggesting that organics and sulfate are likely internally mixed in large particles.

To:

Various studies have analyzed the particle mixing state using single-particle instruments such as the aerosol time-of-flight mass spectrometer (Healy et al., 2013, 2014; Yang et al., 2012) and the single-particle aerosol mass spectrometer (Wang et al., 2015). Particle mixing state can also be inferred from particle size information obtained with the AMS. If the organics and sulfate are internally mixed (i.e. they exist in the same particle), their diameters should be strongly correlated with each other and their size should grow at a similar rate. The observed strong correlation and slope of unity (correlated in time and size) suggest that these species are likely internally mixed, although we cannot completely exclude the possibility of external mixing. On the other hand, if the mode diameters of sulfate and organics did not change coherently and exhibit a strong correlation with a slope close to unity, these particles were more likely externally mixed. Bahreini et al. (2003) have used such correlations in size to indicate the mixing states of species. In our study, the large mode diameters of organics and sulfate were strongly correlated (Pearson's R value equals 0.7) with a slope close to unity in LWC episodes (Figure 5), suggesting that organics and sulfate were likely internally mixed in the large particles. However, these conditions of correlation and slope are necessary but not sufficient evidence for internal mixing.

4. Page 9, Line 199: Does the authors consider that fraction of sulfate was higher in LWC episodes (56%)

than the other episodes because of efficient aqueous oxidation?

Although the fraction of sulfate was higher in LWC episodes than in other episodes (LWC: 56%, IR:49%, and LRT: 45%), the absolute mass concentrations of sulfate were quite similar (LWC: $12.4 \mu\text{g m}^{-3}$, IR: $11.7 \mu\text{g m}^{-3}$ and LRT: $11.8 \mu\text{g m}^{-3}$). Aqueous oxidation is considered to be important in LWC episodes, when the aerosol liquid water content was relatively high and solar irradiance was quite low (Table 1). However, we did not aim to compare the efficiency of different pathways of sulfate formation under different conditions. We apologized that we may have confused the reviewer in the manuscript.

5. Page 10, Line 214-217: Please clarify how the percentages were estimated. In Fig. 5, the range of sulfate particle diameter seems to be smaller in IR episodes than LWC episodes.

The percentage numbers were calculated by comparing the smallest diameter in the blue shaded area and the largest diameter in the orange shaded area in each episode. Then, the percentage changes were averaged in each episode type. For example, there are two episodes in the LWC episode type, and the percentage changes for mode diameters in these two episodes were averaged to obtain the percentage changes for the LWC episode type.

The small range of sulfate particle diameter in Figure 5 is because only data points DURING the episodes were plotted. The size variation DURING the episodes were less obvious compared to days BEFORE the episodes (as illustrated in Line 222 of the manuscript). Please also refer to our response to Comment #4 of Reviewer 1.

Change from:

Figure 6 shows that, in the two LWC episodes, the size variations for both the small and large modes were less obvious: -2.5% for organics small mode, +8.1% for organics large mode, +1.6% for sulfate small mode, and -3% for sulfate large mode from start to end as shown in the figure. By contrast, the size variations in the IR episodes were much more drastic: +51.3% for organics small mode, +40.5% for organics large mode, +45.4% for sulfate small mode, and +35.9% for sulfate large mode.

To:

Figure 6 shows the particle mass mode diameters and areas (concentrations) in the LWC and IR types of episodes. We obtained the percentage changes in mode diameters by comparing the smallest diameter before the episode and the largest diameter during the episode for each episode. These percentages in

each episode was then averaged to obtain the percentage changes for each episode type. The results show that the changes in mode diameter were small in the LWC episodes: -2.5% for small mode organics, +8.1% for large mode organics, +1.6% for small mode sulfate, and -3% for large mode sulfate. In contrast, the changes in mode diameters changes were much more drastic in the IR episodes: +51.3% for small mode organics, +40.5% for large mode organics, +45.4% for small mode sulfate, and +35.9% for large mode sulfate. Furthermore, particle size usually increased more rapidly before the IR episodes (shaded in blue in Figure 6) than during the episodes (shaded in orange).

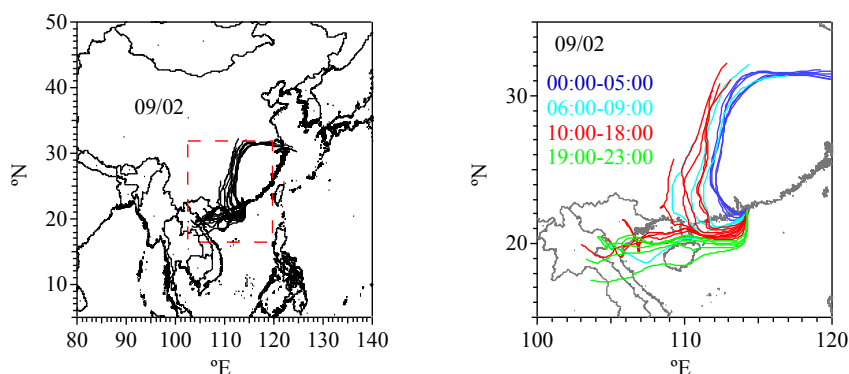
6. Page 10, Line 235: Can discussion on the “typical” IR episode (E4) be generally applicable to the other four IR episodes in different season? Although temporal variation patterns in E4 may be similar to those in Fig. 2b, temporal variation patterns and ratio of LVOOA: SVOOA seems to be quite different from one IR episode to another (Fig. S4).

It was a mistake that we describe E4 as “typical”. It is corrected in the revised manuscript.

We chose E4 for a detailed study because of its land-sea breeze wind pattern and the low wind speeds, which provide a relatively stagnant condition with less influence of transported pollutants for a close examination of in-situ photochemical evolution. Although other IR episodes had high solar irradiance, they are complicated by regional transport effects. It is not appropriate to directly apply all the conclusions from E4 to the other IR episodes.

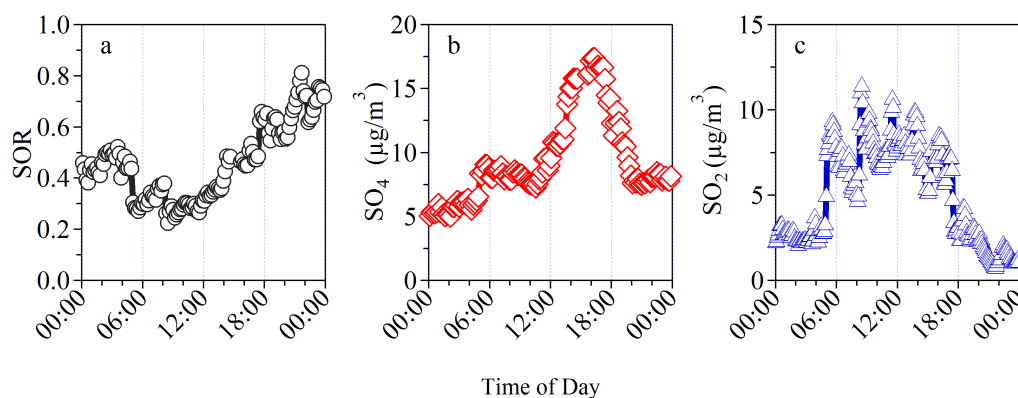
7. Page 10, Line 238-243: Does this mean that 72-h backward trajectory-based air mass origin could not explain the ground-level pollution, or the trajectories (at least for the first 24h) reflected a land-sea breeze pattern?

We used the overall trajectory analysis and further clustering to distinguish air masses into long-, medium-, and short-range transport patterns in groups. It is difficult to reflect a land-sea breeze pattern from these analyses. Rather, a detailed examination of the hourly backward trajectories during E4 (as below) shows that the air mass shifted from inland region to oceanic region, reflecting the land-sea breeze pattern. See figures below.



8. Page 11, Line 274-277: SOR was the maximum after 18:00 on the day. Is SOR appropriate indicator of the photochemical SO₂ conversion?

The sulfur conversion ratio has been widely used to examine the atmospheric formation of particulate sulfur oxidation products from SO₂ (Khoder, 2002; Lee et al., 2015; Miyakawa et al., 2007; Squizzato et al., 2013; Sun et al., 2006; Wang et al., 2005). SOR was at maximum after 18:00 because of the low level of SO₂ gas. During daytime, especially from 10:00 to 18:00, particle-phase sulfate increased while SO₂ decreased. Moreover, the increases in SOR coincided with the increase in the ratio of benzene to toluene (Figure 9c), which is an indication of photochemical age. Sulfate/ Δ CO ratio also increased as photochemical age increased (Figure 10). We consider SOR an appropriate indicator of photochemical conversion of SO₂ in this analysis.



9. Technical corrections: Page 6, Line 129: “benzenze” => “benzene”

Changed as suggested.

10. Page 10, Line 224-232: “3.4. Frequency of high PM1 episodes” can be moved into “3.1. Meteorological conditions and classification of episodes”.

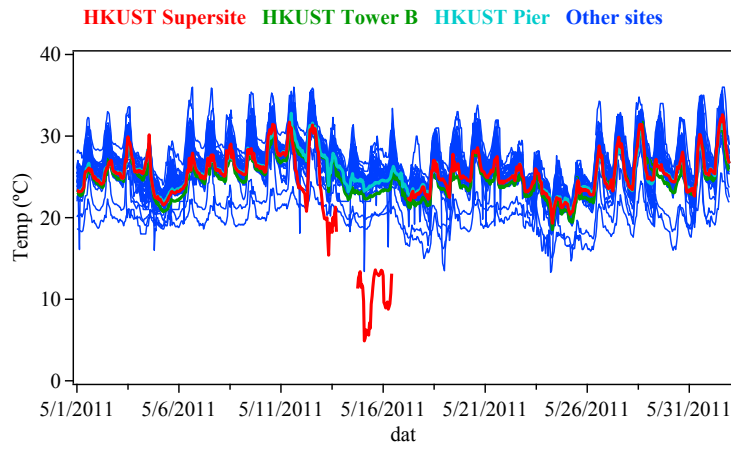
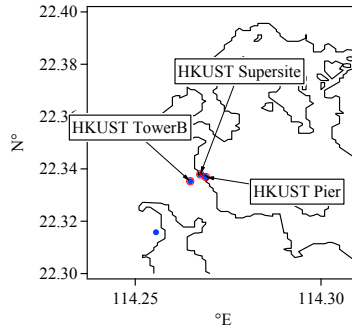
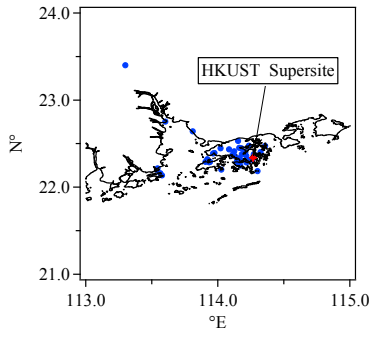
Changed as suggested.

11. Page 13, Line 313: “corresonding” => “corresponding”

Changed as suggested.

12. Fig. S4: Why pressure decreases with increasing mixing height? It is hard to believe that pressure was frequently less than 900 hPa at the ground-level of the study site. Air temperature in 05/14-05/16 episode seems to be quite low. Is it correct? Please provide time series of gaseous species other than OX (i.e., CO, SO₂ and NO_x).

The pressure we used was the average pressure in the boundary layer, not the surface pressure. We have removed the pressure in the revised manuscript. After comparison with other data, we indeed found that there is a deviation of the HKUST supersite temperature with the other temperature measurements within this region. We have changed the temperature data from HKUST supersite to the temperature data from an adjacent site (HKUST pier, 100 m away) as shown below. We have also added the time series of gaseous species (CO, NO_x, SO₂, and O_x) in the revised supplementary information.



Reference:

Bahreini, R., Jimenez, J. L., Wang, J., Flagan, R. C., Seinfeld, J. H., Jayne, J. T. and Worsnop, D. R.: Aircraft-based aerosol size and composition measurements during ACE-Asia using an Aerodyne aerosol mass spectrometer, *J. Geophys. Res.*, 108(D23), 8645, doi:10.1029/2002JD003226, 2003.

Cheung, H. H. Y., Tan, H., Xu, H., Li, F., Wu, C., Yu, J. Z. and Chan, C. K.: Measurements of non-volatile aerosols with a VTDMA and their correlations with carbonaceous aerosols in Guangzhou, China, *Atmos. Chem. Phys.*, 16(13), 8431–8446, doi:10.5194/acp-16-8431-2016, 2016.

Huang, D. D., Li, Y. J., Lee, B. P. and Chan, C. K.: Analysis of Organic Sulfur Compounds in Atmospheric Aerosols at the HKUST Supersite in Hong Kong Using HR-ToF-AMS, *Environ. Sci. Technol.*, 150305134049007, doi:10.1021/es5056269, 2015.

Huang, X. H. H., Bian, Q., Ng, W. M., Louie, P. K. K. and Yu, J. Z.: Characterization of PM_{2.5} major components and source investigation in suburban Hong Kong: A one year monitoring study, *Aerosol Air Qual. Res.*, 14(1), 237–250, doi:10.4209/aaqr.2013.01.0020, 2014.

Khoder, M. I.: Atmospheric conversion of sulfur dioxide to particulate sulfate and nitrogen dioxide to particulate nitrate and gaseous nitric acid in an urban area, *Chemosphere*, 49(6), 675–684, doi:10.1016/S0045-6535(02)00391-0, 2002.

Lee, B. P., Li, Y. J., Yu, J. Z., Louie, P. K. K. and Chan, C. K.: Physical and chemical characterization of ambient aerosol by HR-ToF-AMS at a suburban site in Hong Kong during springtime 2011, *J. Geophys. Res. Atmos.*, 118(15), 8625–8639, doi:10.1002/jgrd.50658, 2013.

Lee, B. P., Li, Y. J., Yu, J. Z., Louie, P. K. K. and Chan, C. K.: *Journal of Geophysical Research : Atmospheres*, , 1–19, doi:10.1002/2015JD023311.Received, 2015.

Li, Y. J., Lee, B. Y. L., Yu, J. Z., Ng, N. L. and Chan, C. K.: Evaluating the degree of oxygenation of organic aerosol during foggy and hazy days in Hong Kong using high-resolution time-of-flight aerosol mass spectrometry (HR-ToF-AMS), *Atmos. Chem. Phys.*, 13(17), 8739–8753, doi:10.5194/acp-13-8739-2013, 2013.

Li, Y. J., Lee, B. P., Su, L., Fung, J. C. H. and Chan, C. K.: Seasonal characteristics of fine particulate

matter (PM) based on high-resolution time-of-flight aerosol mass spectrometric (HR-ToF-AMS) measurements at the HKUST Supersite in Hong Kong, *Atmos. Chem. Phys.*, 15(1), 37–53, doi:10.5194/acp-15-37-2015, 2015.

Meng, J. W., Yeung, M. C., Li, Y. J., Lee, B. Y. L. and Chan, C. K.: Size-resolved cloud condensation nuclei (CCN) activity and closure analysis at the HKUST Supersite in Hong Kong, *Atmos. Chem. Phys.*, 14(18), 10267–10282, doi:10.5194/acp-14-10267-2014, 2014.

Miyakawa, T., Takegawa, N. and Kondo, Y.: Removal of sulfur dioxide and formation of sulfate aerosol in Tokyo, *J. Geophys. Res. Atmos.*, 112(13), 1–13, doi:10.1029/2006JD007896, 2007.

Squizzato, S., Masiol, M., Brunelli, a., Pistollato, S., Tarabotti, E., Rampazzo, G. and Pavoni, B.: Factors determining the formation of secondary inorganic aerosol: A case study in the Po Valley (Italy), *Atmos. Chem. Phys.*, 13(4), 1927–1939, doi:10.5194/acp-13-1927-2013, 2013.

Sun, Y., Zhuang, G., Tang, A., Wang, Y. and An, Z.: Chemical Characteristics of PM 2.5 and PM 10 in Haze–Fog Episodes in Beijing, *Environ. Sci. Technol.*, 40(10), 3148–3155, doi:10.1021/es051533g, 2006.

Wang, Y., Zhuang, G., Tang, A., Yuan, H., Sun, Y., Chen, S. and Zheng, A.: The ion chemistry and the source of PM_{2.5} aerosol in Beijing, *Atmos. Environ.*, 39(21), 3771–3784, doi:10.1016/j.atmosenv.2005.03.013, 2005.

Yeung, M. C., Lee, B. P., Li, Y. J. and Chan, C. K.: Simultaneous HTDMA and HR-ToF-AMS measurements at the HKUST Supersite in Hong Kong in 2011, *J. Geophys. Res. Atmos.*, 119(16), 9864–9883, doi:10.1002/2013JD021146, 2014.

Particulate matter (PM) episodes at a suburban site in Hong Kong: evolution of PM characteristics and role of photochemistry in secondary aerosol formation

Yi Ming Qin¹, Yong Jie Li^{2,*}, Hao Wang³, Berto Paul Yok Long Lee³, Dan Dan Huang¹, and Chak Keung Chan^{1,3,4,*}

¹Department of Chemical and Biomolecular Engineering, Hong Kong University of Science and Technology, Hong Kong, China

²Faculty of Science and Technology, University of Macau, Taipa, Macau, China

³Division of Environment, Hong Kong University of Science and Technology, Hong Kong, China

⁴School of Energy and Environment, City University of Hong Kong, Hong Kong, China

*To Whom Correspondence Should be Addressed

Chak K. Chan: AC1-G5716, School of Energy and Environment, City University of Hong Kong,

Tat Chee Avenue, Kowloon, Hong Kong, China

Tel: (852) 3442-5593; Fax: (852) 3442-0688

Email: chak.k.chan@cityu.edu.hk

Yong Jie Li: E11-3017, Faculty of Science and Technology, University of Macau, E11, Avenida da Universidade,
Taipa, Macau, China

Tel: (853) 8822-4943; Fax: (853) 8822-2426

Email: yongjieli@umac.mo

1 **Abstract**

2 Episodes with high concentrations of particulate matter (PM) across the seasons were investigated during four
3 one-month campaigns at a suburban site in Hong Kong. High-resolution time-of-flight aerosol mass spectrometer
4 (HR-ToF-AMS) measurements revealed that both regional transport and secondary formation contributed to high
5 PM levels during the episodes at this site. Based on distinct meteorological conditions, episodes were categorized
6 into three types: liquid water content (LWC), solar irradiance (IR), and long-range transport (LRT). Despite the
7 difference in meteorological conditions, all episodes were characterized by a high fraction of sulfate (45%-56%) and
8 organics (23%-34%). However, aerosols in LWC episodes were less aged, consisting of the lowest fraction of
9 secondary organics aerosols (SOA) and the highest fraction of small particles. Large particles mixed internally while
10 freshly formed small particles mixed externally in LWC episodes. Aerosols in LRT episodes, by contrast, were the
11 most aged and consisted of the highest proportion of low-volatility oxygenated organic aerosols (LVOOA) and the
12 lowest proportion of small particles. Both small and large particles mixed externally in LRT episodes. The highest
13 proportion of semi-volatile oxygenated organic aerosols (SVOOA) and a medium proportion of small particles were
14 observed in IR episodes. Both small and large particles were likely externally mixed during IR episodes. Unlike in
15 the other two types of episodes, in IR episodes aerosols experienced the most dramatic size increase and diurnal
16 variation, with a time lag between SVOOA and LVOOA and a gradual increase in carbon oxidation state ($\overline{OS}_c \approx$
17 $2 \times O:C-H:C$). Five out of ten episodes were of the IR type, further reflecting the importance of this type of episode.
18 The evolution of aerosol components in one particular episode of the IR type, which exhibited a clear land-sea
19 breeze pattern, was examined in detail. Sulfate and SOA due to photochemical aging were very efficiently produced
20 during the course of six hours. The “~~less-oxidized~~” SOA (SVOOA) was initially formed at a higher rate than the
21 “~~more-oxidized~~” SOA (LVOOA). The SVOOA transformed to LVOOA at the later stage of photochemical aging.
22 This transformation was further supported by mass spectral analysis, which showed an increase in the most oxidized
23 ion (CO_2^+) and decreases in moderately oxidized ones ($C_2H_3O^+$, $C_3H_3O^+$ and $C_3H_5O^+$). By measuring the physical
24 and chemical properties of PM in a highly time-resolved manner, the current study was able to demonstrate the
25 dynamic and complex nature of PM transformation during high-PM episodes.

Deleted: fresh

Deleted: aged

28 **1. Introduction**

29 Hong Kong and the rest of the Pearl River Delta (PRD) in China have been battling air pollution episodes as a
30 result of rapid economic development and urbanization in the region (Ho et al., 2003; Zhong et al., 2013).
31 Meteorological conditions may govern the regional and long-range transport of air pollutants to Hong Kong. For
32 example, northerly winds can bring pollutants from the inland areas to Hong Kong, and have been suggested to be
33 responsible for regional air pollution events in winter (Fang et al., 1999; Huang et al., 2009, 2014b). The majority of
34 earlier studies used filter sampling with a low time resolution of hours to days, and so were unable to track the
35 temporal chemical transformation in high particulate matter (PM) episodes. This limitation has hindered our
36 understanding of the dynamic nature of PM undergoing rapid chemical transformations. Such chemical
37 transformation can occur within short time periods (e.g., within a day), and so do other physicochemical properties
38 such as hygroscopic and optical properties. High-time-resolution chemical characterization techniques, for example
39 the Aerodyne high-resolution time-of-flight aerosol mass spectrometer (HR-ToF-AMS), offer a temporal resolution
40 of a few minutes. These techniques can thus provide valuable information on rapid changes in the PM composition,
41 facilitating more detailed analysis of pollution events (Decarlo et al., 2006). HR-ToF-AMS measurements also give
42 the size distributions of components (DeCarlo et al., 2008; Lee et al., 2013b). These data can reveal the origin,
43 formation and atmospheric processing mechanisms of PM (Seinfeld and Pandis, 2006; Shiraiwa et al., 2013), but
44 they remain under-utilized in most aerosol mass spectrometer (AMS) studies.

45 Secondary formation has been recognized as an important route leading to high PM concentrations worldwide
46 (Zhang et al., 2015a) and is the main culprit for haze episodes in cities across China (Huang et al., 2014a).
47 Secondary organic aerosol (SOA) has been shown to dominate over primary organic aerosol (POA) after a few
48 hours of photochemical aging, for instance, in Mexico City (Decarlo et al., 2010; Volkamer et al., 2006), Pasadena
49 (Hayes et al., 2013) and Tokyo (Takegawa et al., 2006). Semi-volatile oxygenated organic aerosol (SVOOA), which
50 serves as a proxy for ~~less-oxidized~~ SOA, has been shown to transform to low-volatility oxygenated organic aerosol
51 (LVOOA), which serves as a proxy for ~~more-oxidized~~ SOA, in laboratory experiments (Alfarra et al., 2012; Jimenez
52 et al., 2009). Such transformation process may contribute substantially to the accumulation of PM, leading to
53 episodic events that are frequently observed in the fast-developing city clusters in China (Huang et al., 2012; Zhang
54 et al., 2015b).

Deleted: fresh

Deleted: aged

57 We conducted four one-month campaigns in each of the four seasons at the Hong Kong University of Science
58 and Technology (HKUST) Air Quality Research Supersite (AQRS) from May 2011 to February 2012 using an
59 Aerodyne HR-ToF-AMS for non-refractory PM₁ (PM with aerodynamic diameter less than 1 micron). In our
60 previous studies, we found that photochemical oxidation during a haze episode and aqueous-phase reactions during
61 two foggy periods both led to a high degree of oxygenation of organics due to aging in gas phase and/or aqueous
62 phase with substantial SOA formation (Lee et al., 2013 and Li et al., 2013). In spring and summer, SOA, with
63 abundant SVOOA, was more likely to form locally. The oxygen-to-carbon atomic ratio (O:C) and average carbon
64 oxidation state (\overline{OS}_c) peaked in the afternoon in spring and summer (Li et al., 2015). In autumn and winter, LVOOA
65 dominated in SOA. The O:C ratio and \overline{OS}_c showed little diurnal variation. Huang et al. (2015) estimated the
66 contents of organic sulfur compounds in Hong Kong in September 2011. They highlighted the importance of both
67 aqueous-phase processing and regional influence for the formation of organic sulfur compounds. Closure analysis
68 was performed between the PM hygroscopicity measured by a hygroscopic tandem differential mobility analyzer
69 (HTDMA) and chemical composition measured by an HR-ToF-AMS and a constant growth factor of 1.18 for
70 organics was found to be adequate for a good closure, given the dominant contribution of the very hygroscopic
71 sulfate at this suburban site (Cheung et al., 2016; Yeung et al., 2014). Meng et al. (2014) found that the aerosol
72 hygroscopic parameter (k) decreased with an increasing organic-to-inorganic volume ratio. Furthermore, the
73 concentration of cloud condensation nuclei (CCN) was found to be more sensitive to the mixing state and
74 hygroscopicity of the particles at a high supersaturation (SS)=0.70% and a low SS=0.15%, respectively.

75 The above studies primarily focused on the analysis of campaign-average scenarios, without specifically
76 looking at episodic events that occurred during the campaign. In the current study, we investigated the chemical
77 transformation and size evolution of secondary aerosols in high particulate matter episodes across the four seasons.
78 Specifically, we examined in detail the photochemical evolution in a particular episode in which local influences
79 were dominant. Results from the current study reveal the rapid evolution of secondary aerosols and are relevant to
80 other megacities with large precursor input and high photochemical activity.

82 2. Experimental Section

83 2.1. Sampling Site and Measurements

Deleted: We conducted four one-month campaigns in each of the four seasons at the Hong Kong University of Science and Technology (HKUST) Air Quality Research Supersite (AQRS) from May 2011 to February 2012 using an Aerodyne HR-ToF-AMS for non-refractory PM₁ (PM with aerodynamic diameter less than 1 micron). We have previously examined the general characteristics (Lee et al., 2013a; Li et al., 2013, 2015), seasonal trends (Li et al., 2015), aqueous-phase process in the formation of oxygenated organics (Lee et al., 2013a; Li et al., 2013, 2015), organic sulfur compounds (Huang et al., 2015), and particle hygroscopicity (Meng et al., 2014; Yeung et al., 2014). Most of these studies did not explore in detail the evolution of PM characteristics on the timescale of hours. The current work thus focuses on high PM episodes lasting a day or several days across the seasons. Specifically, we aim to investigate the role of local photochemical activity in the formation and evolution of secondary aerosols based on the real-time chemical composition and size distribution data.

103 The sampling periods were from 25 April to 1 June 2011 (spring), from 1 September to 29 September 2011
104 (summer), from 28 October to 15 December 2011 (autumn), and from 19 January to 1 March 2012 (winter). HR-
105 ToF-AMS measurements were conducted at the HKUST AQRS (22°20'N, 114°16'E). The HKUST AQRS is
106 located on the campus of HKUST, which sits on the hillside of Clear Water Bay on the east coast of Hong Kong that
107 has relatively low population density. There is little local emission around the site. Two minor local sources include
108 Clear Water Bay Road and a small student canteen. The Clear Water Bay Road is located outside of the campus and
109 has mild traffic. The student canteen within 200m of the site, which operates only from 18:00LT (local time) until
110 midnight. The HR-ToF-AMS operating procedure, data analysis and species determination have been discussed in
111 Lee et al. (2013a), Li et al. (2015) and Huang et al. (2015). Briefly, the AMS was operated alternatively between the
112 V+PToF combined mode and the W-mode for 5 min each. A collection efficiency of 0.5 was employed for
113 measurements at this site, where the particles have overwhelmingly dominant sulfate content (Aiken et al., 2009; Li
114 et al., 2013). Concentrations of methanesulfonic acid (MSA) and organosulfates (OS) were estimated by combining
115 the V-mode data for total concentrations and the W-mode data for high-resolution mass spectral analysis for specific
116 ions (Huang et al., 2015). Mass spectra of organic sulfur compounds were obtained from standards in laboratory
117 experiments to support the W-mode data analysis (Huang et al., 2015). We further calculated the particle liquid
118 water content (LWC) by applying E-AIM II (Clegg et al., 1998) to explore the effects of aqueous processing on PM₁
119 composition. Gaseous species (CO, CO₂, SO₂, NO, NO₂, and O₃) were measured with standard gas analyzers
120 (Teledyne API). Volatile organic compounds (VOCs) were measured by gas chromatography (Synspec GC955).
121 Meteorological parameters were measured by an automatic weather station mounted on a tower right next to the
122 supersite. Particle hygroscopicity and size distribution measurements have previously been taken with a HR-ToF-
123 AMS at this site (Cheung et al., 2015; Man et al., 2015; Meng et al., 2014; Yeung et al., 2014), and direct reference
124 to the resulting publications will be made where necessary.

125 2.2. Data analysis

126 2.2.1. Criteria for an episodic event

127 The total non-refractory PM₁ (NR-PM₁) concentration showed little seasonal variation, with monthly averages
128 ranging from 14.3 to 15.9 µg m⁻³ as reported by Li et al. (2015). In this work, we defined episodic events according
129 to the following criteria: 1) lasting for at least 24 hours; 2) daily NR-PM₁ average mass concentration exceeding 15

130 $\mu\text{g m}^{-3}$ (overall monthly averaged concentration); and 3) maximum concentration exceeding $30 \mu\text{g m}^{-3}$. According to
131 these criteria, 10 episodic events were identified in the campaigns as shown in Figure S1.

132 **2.2.2. Source apportionment**

133 Following the results in Li et al. (2015), 72-hour backward air trajectory analysis and positive matrix
134 factorization (PMF) analysis were performed. Briefly, the back trajectory analysis was run at an elevation of 300 m
135 using the HYSPLIT-4.8 (Hybrid Single-Particle Lagrangian Integrated Trajectory) model developed by
136 NOAA/ARL (U.S. National Oceanic and Air Administration/Air Resources Laboratory). We classified air masses
137 affecting Hong Kong into long-, medium-, and short-range transport patterns for transport distances of 1000 km,
138 between 500 and 1000 km, and less than 500 km, respectively (Su et al., 2015).

139 For PMF analysis, a four-factor solution with hydrocarbon-like organic aerosols (HOA), cooking organic
140 aerosols (COA), SVOOA, and LVOOA was adopted as in Li et al. (2015). During episodic events, HOA and COA
141 contributed insignificantly (less than 6% and 5% respectively) to total organic aerosol (OA). Since we are interested
142 in SOA transformation, HOA and COA were combined into one POA factor in the following discussion.

143 **2.2.3. Size distribution**

144 Size distributions of aerosol species are obtained with the HR-ToF-AMS when a set of pre-selected m/z is
145 scanned as a function of the particle time of flight. We focus on the size distribution analysis of sulfate and organics
146 because of their overwhelming dominance in NR- PM_{10} . The raw 10-min mass-size distributions of organics and
147 sulfate during the episodic events were averaged over various time periods pertaining to the resolution (e.g. 24 hours,
148 1 hour). The average size distributions were then fitted by the peak fitting tool Multipeak Fit V2 provided by Igor
149 Pro (Wavemetrics) using two log-normal peaks. The peaks were chosen such that the fit residuals were minimized.
150 The two fitted peaks of the size distributions will hereafter be referred to as the small particle mode and the large
151 particle mode. Fitting examples can be found in Figure S2. We will focus on the most important fitting parameters:
152 the particle mass-mode diameter (vacuum aerodynamic diameter, D_{va}) indicating the shift in particle size and the
153 integrated peak areas of the small particle mode and the large particle mode indicating the changes in mass
154 concentrations of larger or smaller particles.

155

156 **2.2.4. Photochemical age**

157 The photochemical age is useful for studying the extent of photochemical processing in an air mass. One way to
158 estimate the photochemical age (Δt) is by the ratio of a less reactive hydrocarbon to a more reactive one (Kleinman,
159 2003):

$$160 \quad \Delta t = \frac{\ln\left(\frac{C_j}{C_i} * \frac{C_{i0}}{C_{j0}}\right)}{(k_i - k_j)[OH]} \quad (1)$$

161 in which C_i and C_j are concentrations of hydrocarbons i and j at time t , whereas C_{i0} and C_{j0} are concentrations of
162 hydrocarbons i and j at time 0. The symbols k_i and k_j are their respective rates of reaction with hydroxyl radicals
163 (OH). Hofzumahaus et al. (2009) reported a high average OH concentration of 15×10^6 molecules cm^{-3} around noon
164 in the PRD region, much higher than model predictions. Zhou et al. (2014) used an OH concentration of 5.2×10^6
165 molecules cm^{-3} in their calculation of photochemical age in the PRD region. Lacking definitive estimates, we used a
166 conservative OH concentration of 1.5×10^6 molecule cm^{-3} (Hayes et al., 2013; Mao et al., 2009) for the discussion of
167 oxidation trends in this study. The ratio of benzene to toluene has been widely used (El Haddad et al., 2013) because
168 of their similar emission sources and significantly different rates of reaction with OH radicals ($k_{\text{benzene-OH}} = 1.23 \times 10$
169 12 $\text{cm}^3 \text{ molecule}^{-1} \text{ s}^{-1}$; $k_{\text{toluene-OH}} = 6.0 \times 10^{-12}$ $\text{cm}^3 \text{ molecule}^{-1} \text{ s}^{-1}$ at 298K) (Atkinson Roger, 2000). Because toluene
170 reacts more rapidly with OH radicals than does benzene, it is depleted more quickly, resulting in higher
171 benzene/toluene ratios in aged air masses. However, the photochemical age can deviate when fresh pollutants are
172 added to an aged air mass. Since fresh pollutants were insignificant after 10:00 (i.e. no significant peaks of benzene
173 and toluene after 10:00; see Figure S3), we set the start time at 10:00 for the discussion of photochemical aging.

Deleted: benzene

174 3. Results and Discussion

175 3.1. Meteorological conditions and classification of episodes

176 Table 1 summarizes the meteorological conditions, PM_{10} concentrations, and the estimated LWC in the 10 high
177 PM episodes. All of the episodes involved air masses that originated over East Asia from the north, northeast or
178 northwest of Hong Kong, and swept over part of the PRD region before reaching the site. Seven of the 10 episodes
179 (E1-E7) were characterized by medium-range trajectories and the other three (E8-E10) by long-range trajectories.
180 The individual trajectories are shown in Figure S4. E1 and E2 had much lower solar irradiance (IR) but higher LWC
181 than the other episodes, which distinguished them from the other medium-range transport episodes. Thus, E1 and E2
182 were categorized as episodes of the LWC type (medium-range transport with high LWC and low IR) and the other

Deleted: S3

185 medium-range transport episodes as episodes of the IR type (medium-range transport with high IR and low LWC).
186 Li et al. (2013) referred to E1 and E2 as foggy episodes, while Li et al. (2013) and Lee et al. (2013a) referred to E3
187 as a hazy episode. The long-range transport episodes might be less associated with the local site-specific conditions
188 and were categorized as episodes of the LRT type.

189 High concentrations of PM can have a number of causes, including enhanced primary emissions (Ji et al., 2014),
190 concentrating effects due to a decrease in the height of the planetary boundary layer (Petäjä et al., 2016), regional
191 transport (Huang et al., 2009), as well as active secondary formation (Hayes et al., 2013). Local primary emissions
192 were not very significant at this site, as can be seen from the low contribution of POA (less than 6%) throughout the
193 whole campaign. As an indicator for primary PM, elemental carbon (EC) concentrations in PM_{2.5} filter sampling at
194 this site from March 2011 to February 2012 were also found to be low throughout the year (0.86 ± 0.53
195 $\mu\text{g}/\text{m}^3$)(Huang et al., 2014b). Boundary layer dynamics on the high PM days can be a factor affecting PM
196 concentration, but the effects were likely minimal as the highest concentration was usually observed during the day
197 at higher mixing heights (Figure S5). Therefore, regional transport and active secondary formation would be the
198 most probable causes for the episodic events of high PM concentrations at this suburban site. More detailed
199 meteorological conditions with chemical characteristics in each episode can be found in Figure S5.

200 As is apparent from Table 1, the occurrence of different types of episodes exhibits a seasonal trend. LWC
201 episodes occurred only in spring and LRT episodes only in winter, while IR episodes took place in spring, summer
202 and autumn. This result is consistent with previous results (Huang et al., 2009) in that the frequency of high PM
203 days in Hong Kong had a strong seasonal variation. In winter, the overwhelming northerly wind brings pollutants
204 via long-range transport (Fang et al., 1999). In spring, foggy days with high PM levels are common due to the
205 moisture-laden air masses coming in from the sea and aqueous-phase processing of particulate species (Li et al.,
206 2013). In summer and autumn, however, hazy days are mainly due to high photochemical activities in this
207 subtropical area, resulting in the formation of secondary aerosols (Hu et al., 2008; Zhou et al., 2014).

208 3.2. Chemical characteristics of high PM episodes

209 Figure 1 shows the chemical constituents of NR-PM₁ in the three types of episodes. It is apparent that sulfate
210 dominated in all types of episodes. In Hong Kong, sulfate is largely regarded as a major regional pollutant with little
211 spatial variability, as in the rest of the PRD (Hagler et al., 2006; LOUIE et al., 2005). Nitrate contributed less than 4%

Deleted: S4

Deleted: S4

Formatted: Don't adjust right indent when grid is defined, Space After: 0 pt, Don't adjust space between Latin and Asian text, Don't adjust space between Asian text and numbers

Formatted: Font color: Green

214 in LWC episodes and IR episodes, but more than 7% in LRT episodes. As LRT episodes occurred in wintertime,
215 the higher nitrate concentration was likely driven by gas-particle partitioning of ammonium nitrate to the particle at
216 low temperatures (Seinfeld and Pandis, 2006). Using the PMF-resolved SVOOA and LVOOA as proxies for less-
217 oxidized and more-oxidized SOA respectively (Zhang et al., 2011), more details of OA can be revealed. SVOOA
218 had higher contributions in IR episodes, while LVOOA contributed roughly twice as much as SVOOA did in LRT
219 episodes, because the air mass was already quite aged when reached the site. LVOOA and SVOOA made similar
220 contributions in LWC episodes.

221 Figure 2 shows the diurnal variations of the NR-PM₁ species, PMF-resolved organic factors, as well as O_x
222 (O₃+NO₂) in these three types of episodes. SVOOA and LVOOA as well as O_x increased during the day in IR
223 episodes, with a time lag between SVOOA and LVOOA. A similar time lag was also observed between SVOOA
224 and LVOOA in the Yangtze River Delta (YRD), another fast developing region of China (Huang et al., 2012). These
225 delays may be the result of conversions from fresh SVOOA to aged LVOOA in the afternoon. We explore such a
226 possibility in Section 3.6. SVOOA and LVOOA both exhibit flat diurnal patterns in LWC episodes and LRT
227 episodes.

228 Elemental analysis of OA (ratios of H:C, O:C, N:C, S:C and OM:OC) from the high resolution mass spectra
229 provides useful information to assess OA evolution. Recently, Canagaratna et al. (2015) used an updated (Improved-
230 Ambient) method to estimate O:C and H:C ratios, and reported 27% higher O:C ratios and 11% higher H:C ratios
231 than those estimated using the original (Aiken-Ambient) method. Recalculating the elemental ratios for the
232 September dataset using the updated method shows little difference from those obtained by simply applying the
233 respective factors of 1.27 and 1.11 to the O:C and H:C ratios (Figure S5). Hence, the O:C and H:C ratios in this
234 study were corrected by factors of 1.27 and 1.11, respectively, with Aiken-Ambient values reported in our previous
235 studies. In the Van Krevelen diagram (Heald et al., 2010; Ng et al., 2011) shown in Figure 3a, data points for LWC
236 episodes (blue) fall into a lower O:C region than do the data points for IR (red) and LRT episodes (green). Even
237 though data points for IR episodes and LRT episodes have similar slopes and intercepts in the Van Krevelen
238 diagram, data points for IR episodes had a much wider spread. These trends are also reflected in the diurnal patterns
239 of carbon oxidation state ($\overline{\text{OS}}_c \approx 2 \times \text{O:C-H:C}$) (Kroll et al., 2011) in Figure 3b. The $\overline{\text{OS}}_c$ diurnal pattern in LRT
240 episodes was relatively flat, suggesting that oxidized organics were mostly transported to the site with minor in-situ
241 oxidation. The $\overline{\text{OS}}_c$ in IR episodes gradually increased from 09:00 until 15:00. Similar trends were observed for O_x,

Deleted: fresh

Deleted: aged

244 LVOOA and to a less extent, SVOOA. With all these combined, we believe that the local photochemical processing
245 of OA was more likely at play in IR episodes than the long-range transport of processed aerosols.

246

247 3.3. Size distributions of sulfate and organics

248 Figure 4 shows the peak fitting results of the type-averaged size distributions of organics and sulfate mass. The
249 mass-mode diameters (D_{va}) for both the small and large modes of organics and sulfate did not differ considerably
250 across the episode types (smaller than 5% differences). Within each type of episode, sulfate had a smaller fraction of
251 small particle mode than organics did, indicating that sulfate was relatively aged while organics received
252 contributions from local fresh emissions. LWC episodes received the largest contribution from small mode sulfate
253 because of some local influences whereas LRT episodes received the smallest contribution with relatively little local
254 activities. The oxidation mechanisms, however, might be different. Aqueous phase oxidation may dominate in
255 LWC episodes while photochemical oxidation may dominate in IR episodes.

256 Various studies have analyzed the particle mixing state using single-particle instruments such as the aerosol time-
257 of-flight mass spectrometer (Healy et al., 2013, 2014; Yang et al., 2012) and the single-particle aerosol mass
258 spectrometer (Wang et al., 2015). Particle mixing state can also be inferred from particle size information obtained
259 with the AMS. If the organics and sulfate are internally mixed (i.e. they exist in the same particle), their diameters
260 should be strongly correlated with each other and their size should grow at a similar rate. The observed strong
261 correlation and slope of unity (correlated in time and size) suggest that these species are likely internally mixed,
262 although we cannot completely exclude the possibility of external mixing. On the other hand, if the mode diameters
263 of sulfate and organics did not change coherently and exhibit a strong correlation with a slope close to unity, these
264 particles were more likely externally mixed. Bahreini et al. (2003) have used such correlations in size to indicate the
265 mixing states of species. In our study, the large mode diameters of organics and sulfate were strongly correlated
266 (Pearson's R value equals 0.7) with a slope close to unity in LWC episodes (Figure 5), suggesting that organics and
267 sulfate were likely internally mixed in the large particles. However, these conditions of correlation and slope are
268 necessary but not sufficient evidence for internal mixing. This internal mixing may occur during the process of local
269 aqueous oxidation. In IR episodes, during which local photochemical oxidation may have a more obvious influence,
270 larger particles do not mix well internally (poor correlation between the large mode diameters of organics and

Deleted: Within each type of episode, sulfate had a smaller portion of small particle mode than organics did, indicating that sulfate was mostly aged while local activities resulted in some fresh emissions of organics. LWC episodes had the largest small mode contribution and LRT episodes had the smallest, providing additional support that particles were more aged and large particles dominated in LRT episodes while the proportion of fresher small particles was higher in LWC and IR episodes due to stronger local influences.

Deleted: Various studies have analyzed the particle mixing state based on single-particle instruments such as the aerosol time-of-flight mass spectrometer (Healy et al., 2013, 2014; Yang et al., 2012) and the single-particle aerosol mass spectrometer (Wang et al., 2015). Particle mixing state can also be inferred from particle size information obtained with the AMS. The large mode diameters of organics and sulfate (Pearson's R value equals to 0.7) were strongly correlated with a slope close to unity in LWC episodes (Figure 5), suggesting that organics and sulfate are likely internally mixed in large particles.

Deleted: , which has been thoroughly discussed in Li et al. (2013)

293 sulfate with $R_{pr} = 0.2$). As discussed in Section 3.2, in IR episodes, organics showed a clear noontime peak
294 associated with local photochemical activities while sulfate was still mainly a regional pollutant. As a result, large
295 particles of organics and sulfates were very likely externally mixed during IR episodes. Good correlation ($R_{pr} = 0.7$)
296 with a large deviation of the slope from unity (slope = 0.5) was observed in LRT episodes. As long-range transport
297 is the dominant process causing high PM levels during LRT episodes, organics and sulfate would be brought to the
298 site together, so their large mode diameters tend to be strongly correlated. However, they may have different origins
299 and may also have undergone different aging processes during the course of long-range transport, and thus they
300 would have different mode diameters. The correlations between the small mode diameters of organics and sulfate
301 were notably weaker, with $R_{pr}=0.5$ in LWC episodes, $R_{pr}=0.2$ in IR episodes, and $R_{pr}=0.2$ in LRT episodes,
302 suggesting that freshly formed small particles mixed externally.

303 As discussed earlier, there may be some local atmospheric processing of aerosols in LWC and IR episodes but not in
304 LRT episodes. Therefore, we further explored the mechanisms underlying the atmospheric processing of LWC and
305 IR episodes based on the size variations before and during episodic events. Figure 6 shows the particle mass mode
306 diameters and areas (concentrations) in the LWC and IR types of episodes. We obtained the percentage changes in
307 mode diameters by comparing the smallest diameter before the episode and the largest diameter during the episode
308 for each episode. These percentages in each episode was then averaged to obtain the percentage changes for each
309 episode type. The results show that the changes in mode diameter were small in the LWC episodes: -2.5% for small
310 mode organics, +8.1% for large mode organics, +1.6% for small mode sulfate, and -3% for large mode sulfate. In
311 contrast, the changes in mode diameters changes were much more drastic in the IR episodes: +51.3% for small mode
312 organics, +40.5% for large mode organics, +45.4% for small mode sulfate, and +35.9% for large mode sulfate.
313 Furthermore, particle size usually increased more rapidly before the IR episodes (shaded in blue in Figure 6) than
314 during the episodes (shaded in orange). With fewer pre-existing particles before the episodes, particle growth likely
315 via condensation and reactive uptake of semi-volatile components was more rapid than during the episodes. The
316 number concentration is discussed in detail in SI.

3.4. Local photochemical formation and evolution of PM: A case study

3.4.1. Time series of species during the local photochemical episode

Deleted: .

Formatted: Indent: First line: 0 ch

Deleted: Figure 6 shows that, in the two LWC episodes, the size variations for both the small and large modes were less obvious: -2.5% for organics small mode, +8.1% for organics large mode, +1.6% for sulfate small mode, and -3% for sulfate large mode from start to end as shown in the figure. By contrast, the size variations in the IR episodes were much more drastic: +51.3% for organics small mode, +40.5% for organics large mode, +45.4% for sulfate small mode, and +35.9% for sulfate large mode. Furthermore, particle sizes usually increased more rapidly during the days before the IR episodes (days shaded in blue in Figure 6) than during the actual episodes (days shaded in orange). Since the particles were fresher and smaller during the days before episodes, they grew more rapidly as gas phase semi-volatile components condensed onto the particles. Moreover, the number concentrations of the pre-existing particles (acting as condensation nuclei) were lower before than during the episodes, rendering more rapid size increases before the episodes. .

Formatted: Font color: Green

Deleted: <#>Frequency of high PM1 episodes . [1]

341 Because of the high frequency of occurrence of IR episodes, we chose one IR episode (E4) to examine the
342 evolution of the aerosols with photochemical oxidation. This particular episode (E4) was under the influence of a
343 clear land-sea breeze pattern with weak winds (Figure 7), a typical meteorological phenomenon that affects air
344 pollution dynamics at this coastal city (Lee et al., 2013a). As can be seen from Figure 7, the maximum wind speed
345 was less than 2 m s^{-1} while the average wind speed was approximately 0.5 m s^{-1} . The wind direction changed from
346 northerly to easterly between 06:00 and 10:00 and remained easterly until 20:00, when it changed clockwise from
347 easterly back to northerly. Under such conditions, local photochemical activities can lead to effective production and
348 accumulation of air pollutants. Time series of organics, sulfate, ammonium, nitrate, MSA, OS, PMF-resolved
349 organic factors, some gaseous species, as well as meteorological parameters were analyzed. Most NR-PM₁ species
350 showed clear diurnal variations. Figure 7 shows that organics increased from a roughly constant concentration of 10
351 $\mu\text{g m}^{-3}$ at night until 09:00 to its highest concentration of $16.6 \mu\text{g m}^{-3}$ at 13:00, while sulfate showed a mild increase
352 at 06:00 and then a sharp increase at 10:30 to reach its highest concentration of $17.4 \mu\text{g m}^{-3}$ at 16:00. They were
353 overall consistent with the increasing trend of irradiance, an indicator of photochemical activities, in the afternoon.
354 Nitrate concentration was high ($2.5 \mu\text{g m}^{-3}$) in the morning and started to decrease from 12:30 onwards to reach 0.3
355 $\mu\text{g m}^{-3}$ by 16:00, likely attributable to vertical dilution due to a rise in the height of the planetary boundary layer, or
356 alternatively evaporation of ammonium nitrate at higher temperatures and lower RH values (Seinfeld and Pandis,
357 2006). Wind direction started to change at 20:00, when all the NR-PM₁ species were at their lowest concentrations.
358 POA concentration increased from $2.5 \mu\text{g m}^{-3}$ at 00:00 to about $5 \mu\text{g m}^{-3}$ at 06:00, which might be due to the
359 lowering of the planetary boundary layer. Conversely, expansion of the boundary layer early in the morning could
360 help disperse the POA. The increase in LVOOA lagged behind that in SVOOA. Starting from 06:00, SVOOA
361 concentration increased rapidly and peaked at approximately 13:00, coinciding with the IR peak, possibly due to
362 fresh SOA formation. LVOOA gradually increased from 12:00 and peaked at 14:00, similar to sulfate. The time lag
363 suggests that some conversion from ~~less-oxidized~~ to ~~more-oxidized~~ SOA might have occurred in the afternoon.
364 Evaporation at the elevated temperature of 30°C throughout the afternoon might also have led to the decrease in
365 SVOOA, as with nitrate. The diurnal variation of MSA shows a noontime peak, consistent with the trend of
366 irradiance. In contrast, OS did not show a clear noontime peak, since OS at this site were likely affected by inland
367 transportation (Huang et al., 2015).

368 3.4.2. Changes in size distribution

Deleted: typical

Deleted: Despite the fact that the 72-hour air mass back trajectories (with arriving height of 300 m) reflected medium-range transport, the surface air was quite stagnant as shown by wind speed data collected from the ground station.

Deleted: fresh

Deleted: aged

376 As shown Figure 8, before 06:00, the size distributions of sulfate and organics were both dominated by a mass
377 mode diameter of 500 to 600 nm. During 06:00-09:00, a shoulder at 200 nm appeared in the size distribution of
378 sulfate and in that of organics, indicating some fresh sulfate and organics were formed or emitted (possibly POA).
379 As photochemical reactions proceeded (09:00-18:00), the shoulder of D_{va} at 200 nm became weaker and the size
380 distributions shifted to the larger end. It should be noted that during the whole aging process, the size distributions of
381 organics were broader than those of sulfate since organics were a mixture of numerous constituents from different
382 primary sources and reaction products formed via different atmospheric processes. The shifts in size distribution
383 suggest that secondary aerosol particles with sulfate and organics aged gradually and grew into larger particles.

384 3.4.3. Photochemical production of secondary species

385 We examine the daytime photochemical activity during E4 by looking at the SO_2 oxidation and changes in the
386 degree of oxygenation of particulate organics. The sulfur oxidation ratio (SOR) has been used to evaluate the extent
387 of atmospheric oxidation of SO_2 to sulfate (Squizzato et al., 2013; Wang et al., 2005). Figure 9c shows the increase
388 in SOR from 0.2 at 9:00 to 0.7 at 18:00, indicating an efficient conversion from SO_2 to sulfate during daytime in this
389 episode. Figure 9b shows that the $\overline{\text{OS}}_c$ increased sharply near 11:00. $\overline{\text{OS}}_c$ was high after 18:00 because most of the
390 organics in PM had been converted to highly oxidized organic compounds during the aging process. Indeed, during
391 this period, LVOOA was the dominant OA component (Figure 7). The increases in SOR and $\overline{\text{OS}}_c$ coincided with
392 the increase in the ratio of benzene to toluene (Figure 9). The oxidation of sulfur species and organic species reflects
393 efficient oxidation during this photochemical episode.

394 To semi-quantitatively evaluate the efficiency of SOA and sulfate formation, the changes in $\text{SOA}/\Delta\text{CO}$,
395 $\text{MSA}/\Delta\text{CO}$, and $\text{sulfate}/\Delta\text{CO}$ are plotted in Figure 10 as a function of photochemical age from 10:00 to 18:00. ΔCO ,
396 defined as the measured CO concentration minus the minimum CO concentration (see Figure 7 for the time series of
397 CO), is assumed to be a conservative tracer of urban combustion emissions. The perturbations of CO concentration
398 by photochemical formation from VOC or destruction by OH radicals were thought to be negligible over such a
399 short timescale (less than eight hours) (Griffin et al., 2007). Normalization of species concentrations to the ΔCO
400 concentration is expected to reduce the effect of dilution (Hayes et al., 2013; Zhou et al., 2014).

401 From 10:00 to 18:00, $\text{sulfate}/\Delta\text{CO}$ increased by a factor of 7-8 as photochemical activity increased on a
402 timescale of approximately 6 h, with a formation rate (indicated by the slope of $\text{species}/\Delta\text{CO}$ vs. photochemical age)
403 of approximately $48 \mu\text{g m}^{-3} \text{ppm}^{-1} \text{h}^{-1}$. $\text{MSA}/\Delta\text{CO}$ also increased by a factor of approximately 3 at a rate of $0.05 \mu\text{g}$

Deleted: c

405 $\text{m}^{-3} \text{ppm}^{-1} \text{h}^{-1}$ during photochemical aging. The good correlation of MSA production with the photochemical age
406 suggests that MSA originated from the reaction of gaseous dimethyl sulfide with OH radicals (Barnes et al., 2006).
407 For comparison, Bardouki et al. (2003) also found that MSA and OH radicals covaried over the northeastern coast of
408 Crete. As shown in Figure 10c, SOA/ ΔCO increased by approximately a factor of 2 with the slope of $7.2 \mu\text{g m}^{-3}$
409 $\text{ppm}^{-1} \text{h}^{-1}$ ($8.07 \mu\text{g sm}^{-3} \text{ppm}^{-1} \text{h}^{-1}$). A shallower slope (approximately 4.0 to $4.5 \mu\text{g sm}^{-3} \text{ppm}^{-1} \text{h}^{-1}$) was observed in
410 Pasadena, California from May to June (Hayes et al., 2013) while a similar slope ($6.18 \mu\text{g m}^{-3} \text{ppm}^{-1} \text{h}^{-1}$) was
411 observed in a previous study in Hong Kong in August (Zhou et al., 2014). This indicates that the SOA production in
412 Hong Kong during the local in situ photochemical oxidation in summer is high.

413 More interestingly, SVOOA/ ΔCO increased during the first three hours but decreased slightly after 13:00, even
414 as photochemical age increased. In contrast, LVOOA/ ΔCO increased steadily throughout the whole stage. After
415 photochemical processing for 6 h, LVOOA/ ΔCO increased by approximately a factor of 20, from $2.3 \mu\text{g m}^{-3} \text{ppm}^{-1}$
416 to $49.4 \mu\text{g m}^{-3} \text{ppm}^{-1}$. Even though both SVOOA/ ΔCO and LVOOA/ ΔCO increased in the first stage, they did so at
417 slightly different rates, where SVOOA/ ΔCO increased faster than LVOOA/ ΔCO . This suggests that the production
418 of SVOOA was more efficient than that of LVOOA in the first stage. However, in the later stage of SOA formation,
419 the net productions of SVOOA were negative, which indicates that SVOOA may have photochemically converted to
420 LVOOA. As discussed earlier, the input of POA and VOC was limited to the early morning in our study. SVOOA
421 was consumed more quickly to form LVOOA than was replenished through further production in the late afternoon.
422 The situation where limited precursors exist to replenish fresh SOA (even under strong photochemical activity)
423 might also occur in other non-urban atmospheric environments, and thus may have an implication for OA
424 transformation in general.

425 3.4.4. Mass spectral evolution

426 Figure 11a shows the evolving organic mass spectra during E4 (~~corresponding to the period of photochemical~~
427 aging). Eight spectra at one-hour intervals from 10:00 to 18:00 are shown from top to bottom. Two changes in the
428 mass spectra with photochemical processes were apparent: 1) decreases in the signal intensities of relatively high
429 m/z ions (e.g., m/z 55, 57, 67, 69, etc.), which indicates greater fragmentation (C-C bond cleavage) with
430 photochemical oxidation; and 2) increases in the mass concentrations of ions having m/z values of 28 (mainly CO^+)
431 and 44 (mainly CO_2^+), which presumably come from aldehyde, ketone and carboxylic acid (Ng et al., 2011). These
432 changes are also reflected in the relative intensity changes of hydrocarbon-like and oxygen-containing ions such as

Deleted: corresponding

434 $C_4H_7^+$, $C_2H_3O^+$ and CO_2^+ (Figure 11b, c). The fractions of tracers of primary organic aerosols $C_3H_7^+$ (m/z 43), $C_4H_7^+$
435 (m/z 55) and $C_4H_9^+$ (m/z 57) (Lambe et al., 2012) decreased. On the other hand, ion fractions of $C_2H_3O^+$ (m/z 43),
436 $C_3H_3O^+$ (m/z 55) and $C_3H_5O^+$ (m/z 57) increased until 13:00 (corresponding to the peak of SVOOA), followed by
437 the decrease of these moderately oxygenated ions. These ions are predominantly from non-acid oxygenates, and are
438 usually associated with less-oxidized SOA. However, The most oxidized ions, CO_2^+ (m/z 44), which is thought to be
439 the marker of more-oxidized SOA, increased continuously. As a result, the mass spectra, which were initially
440 SVOOA-like, evolved to become LVOOA-like with increasing photochemical age (Figure 11d). Overall, this
441 spectral analysis indicates increasingly oxidized organics, as long carbon chains became more functionalized and
442 fragmented after extensive oxidation (Alfarra et al., 2012; Kroll et al., 2009). Such an observation implies efficient
443 transformation of OA within a few hours of photochemical aging, a timescale that could be relevant to chemical
444 transport models concerning SOA formation.

445 4. Conclusion

446 High-resolution HR-ToF-AMS measurements were taken during four one-month campaigns in suburban Hong
447 Kong to illustrate the evolution of high PM episodic events across the seasons. Three types of episodes, medium-
448 range transport with high particle liquid water content (LWC episodes), medium-range transport with high solar
449 irradiance (IR episodes), and long-range transport (LRT episodes), were captured based on synoptic meteorological
450 conditions. Which type of episode occurred depended on the season, with LWC episodes occurring only in spring
451 and LRT episodes only in winter, while IR episodes took place throughout the year except in winter. Sulfate was the
452 major constituent of NR-PM₁ during all episodic events. The contribution of secondary organic species, including
453 SVOOA and LVOOA, varied across episode types, with more SVOOA in the IR episodes and more LVOOA in the
454 LRT episodes. Unlike in the other two types of episodes, in IR episodes organics experienced the most dramatic
455 diurnal variation, with a time lag between SVOOA and LVOOA. This variation was associated with Ox, indicating
456 the conversions from less-oxidized to more-oxidized SOA under photochemical oxidation. Elemental analysis
457 involving the Van Krevelen diagram and carbon oxidation state ($\overline{OS}_c \approx 2 \times O:C-H:C$) further showed that organics in
458 IR were gradually oxidized.

459 Fitted mass-mode diameters for both the small and the large mode of organics remained roughly constant across
460 episode types, while sulfate had a constant small mode diameter in all three types of episodes but a slightly
461 increased large mode diameter in IR episodes. The fraction of small particles decreased from LWC episodes to IR

Deleted: fresh

Deleted: aged

Deleted: fresh

Deleted: aged

466 episodes then to LRT episodes, suggesting that aerosols from long-range transport were more aged and dominated
467 by large particles while episodes under a greater influence of local processes had a higher proportion of fresher
468 small particles. Large particles mixed internally only in LWC episodes, and were more likely to mix externally in IR
469 and LRT episodes. Freshly formed small particles mixed externally in all types of episodes. In IR episodes, aerosols
470 underwent an obvious size increase, while in LWC episodes, the size increase was much less drastic.

471 Because of the high frequency of IR episodes, we picked one particular IR episode featuring land-sea breeze to
472 examine in detail the evolution of aerosol components. Photochemical aging led to mode size shifting for sulfate and
473 organics, indicating particle growth. Increases in the sulfur oxidation ratio and carbon oxidation state were also
474 observed as the aerosols became more aged, which indicates that secondary inorganic species sulfate and SOA were
475 very efficiently produced within six hours of photochemical aging. In the earlier stage of aging, "~~less-oxidized~~"
476 SOA—SVOOA—was formed at a higher rate than "~~more-oxidized~~". SOA—LVOOA. SVOOA clearly transformed
477 to LVOOA at the later stage of photochemical aging, resulting in a 20-fold increase in LVOOA. This conversion
478 was further supported by mass spectral analysis, which showed an increase in the most oxidized ion (CO_2^+) and
479 decreases in moderately oxidized ones ($\text{C}_2\text{H}_3\text{O}^+$, $\text{C}_3\text{H}_3\text{O}^+$ and $\text{C}_3\text{H}_5\text{O}^+$). With real-time size-resolved chemical
480 composition data, we demonstrated that aerosol components can transform very efficiently in just a few hours, a
481 process that is essential in understanding the dynamic nature of aerosol evolution during episodes with high PM
482 concentrations.

483 Acknowledgements

484 This work was supported by the Environmental Conservation Fund of Hong Kong (project number ECWW09EG04)
485 and the Research Grants Council of the Hong Kong Special Administrative Region, China (General Research Fund
486 600413). Y.J. Li gratefully acknowledges the support from the Start-up Research Grant (SRG2015-00052-FST) of
487 the University of Macau. The grant from the HKUST Asian Future Leaders Scholarship Program (AFLSP) is also
488 gratefully acknowledged.

489

490

491

492

Deleted: fresh

Deleted: aged

Deleted: .

496 **References**

- 497 Aiken, A. C., Salcedo, D., Cubison, M. J., Huffman, J. A., DeCarlo, P. F., Ulbrich, I. M., Docherty, K. S., Sueper,
498 D., Kimmel, J. R., Worsnop, D. R., Trimborn, A., Northway, M., Stone, E. A., Schauer, J. J., Volkamer, R. M.,
499 Fortner, E., de Foy, B., Wang, J., Laskin, A., Shutthanandan, V., Zheng, J., Zhang, R., Gaffney, J., Marley, N. A.,
500 Paredes-Miranda, G., Arnott, W. P., Molina, L. T., Sosa, G. and Jimenez, J. L.: Mexico City aerosol analysis during
501 MILAGRO using high resolution aerosol mass spectrometry at the urban supersite (T0) – Part 1: Fine particle
502 composition and organic source apportionment, *Atmos. Chem. Phys.*, 9(17), 6633–6653, doi:10.5194/acp-9-6633-
503 2009, 2009.
- 504 Alfara, M. R., Hamilton, J. F., Wyche, K. P., Good, N., Ward, M. W., Carr, T., Barley, M. H., Monks, P. S., Jenkin,
505 M. E., Lewis, A. C. and McFiggans, G. B.: The effect of photochemical ageing and initial precursor concentration
506 on the composition and hygroscopic properties of β -caryophyllene secondary organic aerosol, *Atmos. Chem. Phys.*,
507 12(14), 6417–6436, doi:10.5194/acp-12-6417-2012, 2012.
- 508 Atkinson Roger, J. A.: Atmospheric degradation of volatile methyl-silicon compounds, *Environ. Sci. Technol.*,
509 34(10), 1970–1976, doi:10.1021/es9910053, 2000.
- 510 Bardouki, H., Berresheim, H., Vrekoussis, M., Sciare, J., Kouvarakis, G., Oikonomou, K., Schneider, J. and
511 Mihalopoulos, N.: Gaseous (DMS, MSA, SO₂, H₂SO₄ and DMSO) and particulate (sulfate and methanesulfonate)
512 sulfur species over the northeastern coast of Crete, *Atmos. Chem. Phys.*, 3(5), 1871–1886, doi:10.5194/acp-3-1871-
513 2003, 2003.
- 514 Barnes, I., Hjorth, J. and Mihalopoulos, N.: Dimethyl sulfide and dimethyl sulfoxide and their oxidation in the
515 atmosphere, *Chem. Rev.*, 106(3), 940–975, doi:10.1021/cr020529+, 2006.
- 516 Canagaratna, M. R., Jimenez, J. L., Kroll, J. H., Chen, Q., Kessler, S. H., Massoli, P., Hildebrandt Ruiz, L., Fortner,
517 E., Williams, L. R., Wilson, K. R., Surratt, J. D., Donahue, N. M., Jayne, J. T. and Worsnop, D. R.: Elemental ratio
518 measurements of organic compounds using aerosol mass spectrometry: characterization, improved calibration, and
519 implications, *Atmos. Chem. Phys.*, 15(1), 253–272, doi:10.5194/acp-15-253-2015, 2015.
- 520 Cheung, H. H. Y., Yeung, M. C., Li, Y. J., Lee, B. P. and Chan, C. K.: Relative Humidity-Dependent HTDMA
521 Measurements of Ambient Aerosols at the HKUST Supersite in Hong Kong, China, *Aerosol Sci. Technol.*, 49(8),
522 643–654, doi:10.1080/02786826.2015.1058482, 2015.
- 523 Cheung, H. H. Y., Tan, H., Xu, H., Li, F., Wu, C., Yu, J. Z. and Chan, C. K.: Measurements of non-volatile aerosols
524 with a VTDMA and their correlations with carbonaceous aerosols in Guangzhou, China, *Atmos. Chem. Phys.*,
525 16(13), 8431–8446, doi:10.5194/acp-16-8431-2016, 2016.
- 526 Clegg, S. L., Brimblecombe, P. and Wexler, A. S.: Thermodynamic Model of the System $\text{H}^+ - \text{NH}_4^+ - \text{Na}^+ - \text{SO}_4^{2-} - \text{NO}_3^- - \text{Cl}^- - \text{H}_2\text{O}$
527 at 298.15 K, *J. Phys. Chem. A*, 102(12), 2155–2171, doi:10.1021/jp973043j, 1998.
- 528 Decarlo, P. F., Kimmel, J. R., Trimborn, A., Northway, M. J., Jayne, J. T., Aiken, A. C., Gonin, M., Fuhrer, K.,
529 Horvath, T., Docherty, K. S., Worsnop, D. R. and Jimenez, J. L.: Field-Deployable, High-Resolution, Time-of-
530 Flight Aerosol Mass Spectrometer, *Anal. Chem.*, 78(24), 8281–8289, doi:10.1029/2001JD001213, Analytical,
531 2006.
- 532 DeCarlo, P. F., Dunlea, E. J., Kimmel, J. R., Aiken, a. C., Sueper, D., Crouse, J., Wennberg, P. O., Emmons, L.,
533 Shinozuka, Y., Clarke, a., Zhou, J., Tomlinson, J., Collins, D. R., Knapp, D., Weinheimer, A. J., Montzka, D. D.,
534 Campos, T. and Jimenez, J. L.: Fast airborne aerosol size and chemistry measurements above Mexico City and
535 Central Mexico during the MILAGRO campaign, *Atmos. Chem. Phys.*, 8(14), 4027–4048, doi:10.5194/acp-8-4027-
536 2008, 2008.
- 537 Decarlo, P. F., Ulbrich, I. M., Crouse, J., De Foy, B., Dunlea, E. J., Aiken, a. C., Knapp, D., Weinheimer, A. J.,
538 Campos, T., Wennberg, P. O. and Jimenez, J. L.: Investigation of the sources and processing of organic aerosol over
539 the Central Mexican Plateau from aircraft measurements during MILAGRO, *Atmos. Chem. Phys.*, 10(12), 5257–
540 5280, doi:10.5194/acp-10-5257-2010, 2010.
- 541 Fang, M., Zheng, M., Wang, F., Chim, K. and Kot, S.: The long-range transport of aerosols from northern China to
542 Hong Kong - a multi-technique study, *Atmos. Environ.*, 33(11), 1803–1817 [online] Available from:
543 <http://repository.ust.hk/ir/Record/1783.1-28286> (Accessed 9 November 2015), 1999.

544 Griffin, R. J., Chen, J., Carmody, K., Vutukuru, S. and Dabdub, D.: Contribution of gas phase oxidation of volatile
545 organic compounds to atmospheric carbon monoxide levels in two areas of the United States, *J. Geophys. Res.*,
546 112(D10), D10S17, doi:10.1029/2006JD007602, 2007.

547 El Haddad, I., D'Anna, B., Temime-Roussel, B., Nicolas, M., Boreave, a., Favez, O., Voisin, D., Sciare, J., George,
548 C., Jaffrezo, J.-L., Wortham, H. and Marchand, N.: Towards a better understanding of the origins, chemical
549 composition and aging of oxygenated organic aerosols: case study of a Mediterranean industrialized environment,
550 *Marseille, Atmos. Chem. Phys.*, 13(15), 7875–7894, doi:10.5194/acp-13-7875-2013, 2013.

551 Hagler, G. S. W., Bergin, M. H., Salmon, L. G., Yu, J. Z., Wan, E. C. H., Zheng, M., Zeng, L. M., Kiang, C. S.,
552 Zhang, Y. H., Lau, A. K. H. and Schauer, J. J.: Source areas and chemical composition of fine particulate matter in
553 the Pearl River Delta region of China, *Atmos. Environ.*, 40(20), 3802–3815, doi:10.1016/j.atmosenv.2006.02.032,
554 2006.

555 Hayes, P. L., Ortega, a. M., Cubison, M. J., Froyd, K. D., Zhao, Y., Cliff, S. S., Hu, W. W., Toohey, D. W., Flynn, J.
556 H., Lefter, B. L., Grossberg, N., Alvarez, S., Rappenglück, B., Taylor, J. W., Allan, J. D., Holloway, J. S., Gilman, J.
557 B., Kuster, W. C., De Gouw, J. a., Massoli, P., Zhang, X., Liu, J., Weber, R. J., Corrigan, a. L., Russell, L. M.,
558 Isaacman, G., Worton, D. R., Kreisberg, N. M., Goldstein, a. H., Thalman, R., Waxman, E. M., Volkamer, R., Lin,
559 Y. H., Surratt, J. D., Kleindienst, T. E., Offenberg, J. H., Dusanter, S., Griffith, S., Stevens, P. S., Brioude, J.,
560 Angevine, W. M. and Jimenez, J. L.: Organic aerosol composition and sources in Pasadena, California, during the
561 2010 CalNex campaign, *J. Geophys. Res. Atmos.*, 118(16), 9233–9257, doi:10.1002/jgrd.50530, 2013.

562 Heald, C. L., Kroll, J. H., Jimenez, J. L., Docherty, K. S., Decarlo, P. F., Aiken, a. C., Chen, Q., Martin, S. T.,
563 Farmer, D. K. and Artaxo, P.: A simplified description of the evolution of organic aerosol composition in the
564 atmosphere, *Geophys. Res. Lett.*, 37(8), doi:10.1029/2010GL042737, 2010.

565 Ho, K. ., Lee, S. ., Chan, C. K., Yu, J. C., Chow, J. C. and Yao, X. .: Characterization of chemical species in PM2.5
566 and PM10 aerosols in Hong Kong, *Atmos. Environ.*, 37(1), 31–39, doi:10.1016/S1352-2310(02)00804-X, 2003.

567 Hofzumahaus, A., Rohrer, F., Lu, K., Bohn, B., Brauers, T., Chang, C.-C., Fuchs, H., Holland, F., Kita, K., Kondo,
568 Y., Li, X., Lou, S., Shao, M., Zeng, L., Wahner, A. and Zhang, Y.: Amplified trace gas removal in the troposphere.,
569 *Science*, 324(5935), 1702–1704, doi:10.1126/science.1164566, 2009.

570 Hu, D., Bian, Q., Li, T. W. Y., Lau, A. K. H. and Yu, J. Z.: Contributions of isoprene, monoterpenes, β -
571 caryophyllene, and toluene to secondary organic aerosols in Hong Kong during the summer of 2006, *J. Geophys.*
572 *Res. Atmos.*, 113(22), 1–14, doi:10.1029/2008JD010437, 2008.

573 Huang, D. D., Li, Y. J., Lee, B. P. and Chan, C. K.: Analysis of Organic Sulfur Compounds in Atmospheric
574 Aerosols at the HKUST Supersite in Hong Kong Using HR-ToF-AMS, *Environ. Sci. Technol.*, 150305134049007,
575 doi:10.1021/es5056269, 2015.

576 Huang, R.-J., Zhang, Y., Bozzetti, C., Ho, K.-F., Cao, J.-J., Han, Y., Daellenbach, K. R., Slowik, J. G., Platt, S. M.,
577 Canonaco, F., Zotter, P., Wolf, R., Pieber, S. M., Bruns, E. a., Crippa, M., Ciarelli, G., Piazzalunga, A.,
578 Schwikowski, M., Abbaszade, G., Schnelle-Kreis, J., Zimmermann, R., An, Z., Szidat, S., Baltensperger, U.,
579 Haddad, I. El and Prévôt, A. S. H.: High secondary aerosol contribution to particulate pollution during haze events
580 in China, *Nature*, doi:10.1038/nature13774, 2014a.

581 Huang, X.-F. F., Yu, J. Z., Yuan, Z. B., Lau, A. K. H. H. and Louie, P. K. K.: Source analysis of high particulate
582 matter days in Hong Kong, *Atmos. Environ.*, 43(6), 1196–1203, doi:10.1016/j.atmosenv.2008.10.013, 2009.

583 Huang, X. F., He, L. Y., Xue, L., Sun, T. L., Zeng, L. W., Gong, Z. H., Hu, M. and Zhu, T.: Highly time-resolved
584 chemical characterization of atmospheric fine particles during 2010 Shanghai World Expo, *Atmos. Chem. Phys.*,
585 12(11), 4897–4907, doi:10.5194/acp-12-4897-2012, 2012.

586 Huang, X. H. H., Bian, Q., Ng, W. M., Louie, P. K. K. and Yu, J. Z.: Characterization of PM2.5 major components
587 and source investigation in suburban Hong Kong: A one year monitoring study, *Aerosol Air Qual. Res.*, 14(1), 237–
588 250, doi:10.4209/aaqr.2013.01.0020, 2014b.

589 Ji, D., Li, L., Wang, Y., Zhang, J., Cheng, M., Sun, Y., Liu, Z., Wang, L., Tang, G., Hu, B., Chao, N., Wen, T. and
590 Miao, H.: The heaviest particulate air-pollution episodes occurred in northern China in January, 2013: Insights
591 gained from observation, *Atmos. Environ.*, 92, 546–556, doi:10.1016/j.atmosenv.2014.04.048, 2014.

592 Jimenez, J. L., Canagaratna, M. R., Donahue, N. M., Prevot, a S. H., Zhang, Q., Kroll, J. H., DeCarlo, P. F., Allan, J.
593 D., Coe, H., Ng, N. L., Aiken, a C., Docherty, K. S., Ulbrich, I. M., Grieshop, a P., Robinson, a L., Duplissy, J.,
594 Smith, J. D., Wilson, K. R., Lanz, V. a, Hueglin, C., Sun, Y. L., Tian, J., Laaksonen, a, Raatikainen, T., Rautiainen,
595 J., Vaattovaara, P., Ehn, M., Kulmala, M., Tomlinson, J. M., Collins, D. R., Cubison, M. J., Dunlea, E. J., Huffman,
596 J. a, Onasch, T. B., Alfarra, M. R., Williams, P. I., Bower, K., Kondo, Y., Schneider, J., Drewnick, F., Borrmann, S.,
597 Weimer, S., Demerjian, K., Salcedo, D., Cottrell, L., Griffin, R., Takami, a, Miyoshi, T., Hatakeyama, S., Shimono,
598 a, Sun, J. Y., Zhang, Y. M., Dzepina, K., Kimmel, J. R., Sueper, D., Jayne, J. T., Herndon, S. C., Trimborn, a M.,
599 Williams, L. R., Wood, E. C., Middlebrook, a M., Kolb, C. E., Baltensperger, U. and Worsnop, D. R.: Evolution of
600 organic aerosols in the atmosphere., *Science*, 326(5959), 1525–1529, doi:10.1126/science.1180353, 2009.

601 Kleinman, L. I.: Photochemical age determinations in the Phoenix metropolitan area, *J. Geophys. Res.*, 108(D3), 1–
602 14, doi:10.1029/2002JD002621, 2003.

603 Kroll, J. H., Smith, J. D., Che, D. L., Kessler, S. H., Worsnop, D. R. and Wilson, K. R.: Measurement of
604 fragmentation and functionalization pathways in the heterogeneous oxidation of oxidized organic aerosol., *Phys.*
605 *Chem. Chem. Phys.*, 11(36), 8005–14, doi:10.1039/b905289e, 2009.

606 Kroll, J. H., Donahue, N. M., Jimenez, J. L., Kessler, S. H., Canagaratna, M. R., Wilson, K. R., Altieri, K. E.,
607 Mazzoleni, L. R., Wozniak, A. S., Bluhm, H., Mysak, E. R., Smith, J. D., Kolb, C. E. and Worsnop, D. R.: Carbon
608 oxidation state as a metric for describing the chemistry of atmospheric organic aerosol, *Nat. Chem.*, 3(2), 133–139,
609 doi:10.1038/nchem.948, 2011.

610 Lambe, A. T., Onasch, T. B., Croasdale, D. R., Wright, J. P., Martin, A. T., Franklin, J. P., Massoli, P., Kroll, J. H.,
611 Canagaratna, M. R., Brune, W. H., Worsnop, D. R. and Davidovits, P.: Transitions from Functionalization to
612 Fragmentation Reactions of Laboratory Secondary Organic Aerosol (SOA) Generated from the OH Oxidation of
613 Alkane Precursors, *Environ. Sci. Technol.*, 46(10), 5430–5437, doi:Doi 10.1021/Es300274t, 2012.

614 Lee, B. P., Li, Y. J., Yu, J. Z., Louie, P. K. K. and Chan, C. K.: Physical and chemical characterization of ambient
615 aerosol by HR-ToF-AMS at a suburban site in Hong Kong during springtime 2011, *J. Geophys. Res. Atmos.*,
616 118(15), 8625–8639, doi:10.1002/jgrd.50658, 2013a.

617 Lee, B. P., Li, Y. J., Flagan, R. C., Lo, C. and Chan, C. K.: Sizing Characterization of the Fast-Mobility Particle
618 Sizer (FMPS) Against SMPS and HR-ToF-AMS, *Aerosol Sci. Technol.*, 47(9), 1030–1037,
619 doi:10.1080/02786826.2013.810809, 2013b.

620 Li, Y. J., Lee, B. Y. L., Yu, J. Z., Ng, N. L. and Chan, C. K.: Evaluating the degree of oxygenation of organic
621 aerosol during foggy and hazy days in Hong Kong using high-resolution time-of-flight aerosol mass spectrometry
622 (HR-ToF-AMS), *Atmos. Chem. Phys.*, 13(17), 8739–8753, doi:10.5194/acp-13-8739-2013, 2013.

623 Li, Y. J., Lee, B. P., Su, L., Fung, J. C. H. and Chan, C. K.: Seasonal characteristics of fine particulate matter (PM)
624 based on high-resolution time-of-flight aerosol mass spectrometric (HR-ToF-AMS) measurements at the HKUST
625 Supersite in Hong Kong, *Atmos. Chem. Phys.*, 15(1), 37–53, doi:10.5194/acp-15-37-2015, 2015.

626 LOUIE, P., WATSON, J., CHOW, J., CHEN, A., SIN, D. and LAU, A.: Seasonal characteristics and regional
627 transport of PM in Hong Kong, *Atmos. Environ.*, 39(9), 1695–1710, doi:10.1016/j.atmosenv.2004.11.017, 2005.

628 Man, H., Zhu, Y., Ji, F., Yao, X., Lau, N. T., Li, Y., Lee, B. P. and Chan, C. K.: Comparison of daytime and
629 nighttime new particle growth at the HKUST supersite in Hong Kong., *Environ. Sci. Technol.*, 49(12), 7170–8,
630 doi:10.1021/acs.est.5b02143, 2015.

631 Mao, J., Ren, X., Brune, W. H., Olson, J. R., Crawford, J. H., Fried, A., Huey, L. G., Cohen, R. C., Heikes, B.,
632 Singh, H. B., Blake, D. R., Sachse, G. W., Diskin, G. S., Hall, S. R. and Shetter, R. E.: Airborne measurement of
633 OH reactivity during INTEX-B, *Atmos. Chem. Phys.*, 9(1), 163–173, doi:10.5194/acp-9-163-2009, 2009.

634 Meng, J. W., Yeung, M. C., Li, Y. J., Lee, B. Y. L. and Chan, C. K.: Size-resolved cloud condensation nuclei (CCN)
635 activity and closure analysis at the HKUST Supersite in Hong Kong, *Atmos. Chem. Phys.*, 14(18), 10267–10282,
636 doi:10.5194/acp-14-10267-2014, 2014.

637 Mohr, C., DeCarlo, P. F., Heringa, M. F., Chirico, R., Slowik, J. G., Richter, R., Reche, C., Alastuey, A., Querol, X.,
638 Seco, R., Peñuelas, J., Jimenez, J. L., Crippa, M., Zimmermann, R., Baltensperger, U., Prévôt, A. S. H.,
639 Peñuelas, J., Jiménez, J. L., Crippa, M., Zimmermann, R., Baltensperger, U. and Prévôt, A. S. H.: Identification and

640 quantification of organic aerosol from cooking and other sources in Barcelona using aerosol mass spectrometer data,
641 *Atmos. Chem. Phys.*, 12(4), 1649–1665, doi:10.5194/acp-12-1649-2012, 2012.

642 Ng, N. L., Canagaratna, M. R., Jimenez, J. L., Chhabra, P. S., Seinfeld, J. H. and Worsnop, D. R.: Changes in
643 organic aerosol composition with aging inferred from aerosol mass spectra, *Atmos. Chem. Phys.*, 11(13), 6465–
644 6474, doi:10.5194/acp-11-6465-2011, 2011.

645 Petäjä, T., Järvi, L., Kerminen, V.-M., Ding, A. J., Sun, J. N., Nie, W., Kujansuu, J., Virkkula, A., Yang, X., Fu, C.
646 B., Zilitinkevich, S. and Kulmala, M.: Enhanced air pollution via aerosol-boundary layer feedback in China., *Sci.*
647 *Rep.*, 6, 18998, doi:10.1038/srep18998, 2016.

648 Seinfeld, J. H. and Pandis, S. N.: *ATMOSPHERIC From Air Pollution to Climate Change SECOND EDITION.*,
649 2006.

650 Shiraiwa, M., Yee, L. D., Schilling, K. a, Loza, C. L., Craven, J. S., Zuend, A., Ziemann, P. J. and Seinfeld, J. H.:
651 Size distribution dynamics reveal particle-phase chemistry in organic aerosol formation., *Proc. Natl. Acad. Sci. U. S.*
652 *A.*, 110(29), 11746–50, doi:10.1073/pnas.1307501110, 2013.

653 Squizzato, S., Masiol, M., Brunelli, a, Pistollato, S., Tarabotti, E., Rampazzo, G. and Pavoni, B.: Factors
654 determining the formation of secondary inorganic aerosol: A case study in the Po Valley (Italy), *Atmos. Chem.*
655 *Phys.*, 13(4), 1927–1939, doi:10.5194/acp-13-1927-2013, 2013.

656 Su, L., Yuan, Z., Fung, J. C. H. and Lau, A. K. H.: A comparison of HYSPLIT backward trajectories generated from
657 two GDAS datasets, *Sci. Total Environ.*, 506–507, 527–537, doi:10.1016/j.scitotenv.2014.11.072, 2015.

658 Takegawa, N., Miyakawa, T., Kondo, Y., Blake, D. R., Kanaya, Y., Koike, M., Fukuda, M., Komazaki, Y.,
659 Miyazaki, Y., Shimono, a. and Takeuchi, T.: Evolution of submicron organic aerosol in polluted air exported from
660 Tokyo, *Geophys. Res. Lett.*, 33(15), 3–7, doi:10.1029/2006GL025815, 2006.

661 Volkamer, R., Jimenez, J. L., San Martini, F., Dzepina, K., Zhang, Q., Salcedo, D., Molina, L. T., Worsnop, D. R.
662 and Molina, M. J.: Secondary organic aerosol formation from anthropogenic air pollution: Rapid and higher than
663 expected, *Geophys. Res. Lett.*, 33(17), L17811, doi:10.1029/2006GL026899, 2006.

664 Wang, Y., Zhuang, G., Tang, A., Yuan, H., Sun, Y., Chen, S. and Zheng, A.: The ion chemistry and the source of
665 PM_{2.5} aerosol in Beijing, *Atmos. Environ.*, 39(21), 3771–3784, doi:10.1016/j.atmosenv.2005.03.013, 2005.

666 Yeung, M. C., Lee, B. P., Li, Y. J. and Chan, C. K.: Simultaneous HTDMA and HR-ToF-AMS measurements at the
667 HKUST Supersite in Hong Kong in 2011, *J. Geophys. Res. Atmos.*, 119(16), 9864–9883,
668 doi:10.1002/2013JD021146, 2014.

669 Zhang, Q., Jimenez, J. L., Canagaratna, M. R., Ulbrich, I. M., Ng, N. L., Worsnop, D. R. and Sun, Y.:
670 Understanding atmospheric organic aerosols via factor analysis of aerosol mass spectrometry: A review, *Anal.*
671 *Bioanal. Chem.*, 401(10), 3045–3067, doi:10.1007/s00216-011-5355-y, 2011.

672 Zhang, R., Wang, G., Guo, S., Zamora, M. L., Ying, Q., Lin, Y., Wang, W., Hu, M. and Wang, Y.: Formation of
673 Urban Fine Particulate Matter, *Chem. Rev.*, 115(10), 3803–3855, doi:10.1021/acs.chemrev.5b00067, 2015a.

674 Zhang, Y. W., Zhang, X. Y., Zhang, Y. M., Shen, X. J., Sun, J. Y., Ma, Q. L., Yu, X. M., Zhu, J. L., Zhang, L. and
675 Che, H. C.: Significant concentration changes of chemical components of PM₁ in the Yangtze River Delta area of
676 China and the implications for the formation mechanism of heavy haze-fog pollution., *Sci. Total Environ.*, 538, 7–
677 15, doi:10.1016/j.scitotenv.2015.06.104, 2015b.

678 Zhong, L., Louie, P. K. K., Zheng, J., Yuan, Z., Yue, D., Ho, J. W. K. and Lau, A. K. H.: Science–policy interplay:
679 Air quality management in the Pearl River Delta region and Hong Kong, *Atmos. Environ.*, 76, 3–10,
680 doi:10.1016/j.atmosenv.2013.03.012, 2013.

681 Zhou, S., Wang, T., Wang, Z., Li, W., Xu, Z., Wang, X., Yuan, C., Poon, C. N., Louie, P. K. K., Luk, C. W. Y. and
682 Wang, W.: Photochemical evolution of organic aerosols observed in urban plumes from Hong Kong and the Pearl
683 River Delta of China, *Atmos. Environ.*, 88, 219–229, doi:10.1016/j.atmosenv.2014.01.032, 2014.

684

Tables:

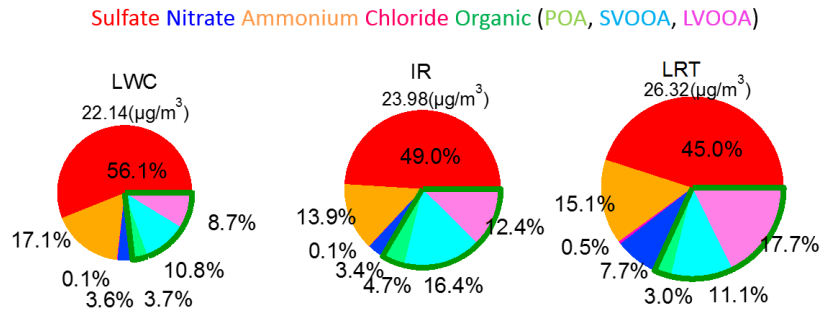
Table 1 Synopsis of meteorological conditions of high PM episodes

Episode	Season	Date	Air mass origin	Wind speed (m s ⁻¹)	Solar Irradiance (w m ⁻²)	Liquid water content (µg m ⁻³)	PM ₁ (µg m ⁻³)	PM ₁ Max (µg m ⁻³)	Type
E1	Spring	28-30 Apr	M-R ^a /NE ^b	0.7±0.4	41±67	47.1±15.9	25.5±3.1	33.1	LWC
E2	Spring	14-16 May	M-R/NE ^b	1.1±0.8	27±61	38.6±14.5	18.8±6.4	32.4	LWC
E3	Spring	27-29 May	M-R ^a /NE ^b	0.9±0.8	184±263	19.3±9.2	28.4±12.6	64.1	IR
E4	Summer	2 Sep	M-R ^a /NW ^b	0.5±0.4	111±163	20.0±3.1	22.5±6.1	33.7	IR
E5	Summer	20-24 Sep	M-R ^a /NE ^b	2.2±0.5	143±234	14.9±4.6	23.8±4.8	35.9	IR
E6	Autumn	3 Nov	M-R ^a /NE ^b	1.3±0.5	174±271	12.8±5.9	15.6±6.2	30.0	IR
E7	Autumn	13-15 Nov	M-R ^a /NE ^b	1.2±0.5	150±221	19.4±7.0	23.4±7.0	45.2	IR
E8	Winter	24-25 Nov	L-R ^a /NE ^b	1.6±0.5	112±174	14.1±6.6	25.9±6.2	38.6	LRT
E9	Winter	8 Feb	L-R ^a /N ^b	2.2±0.6	49±74	27.8±2.8	29.7±8.1	41.6	LRT
E10	Winter	18-19 Feb	L-R ^a /NE ^b	1.5±0.6	104±170	16.0±5.3	25.5±9.4	64.9	LRT

a: Range of air mass origin: Medium range (M-R); Long range (L-R).

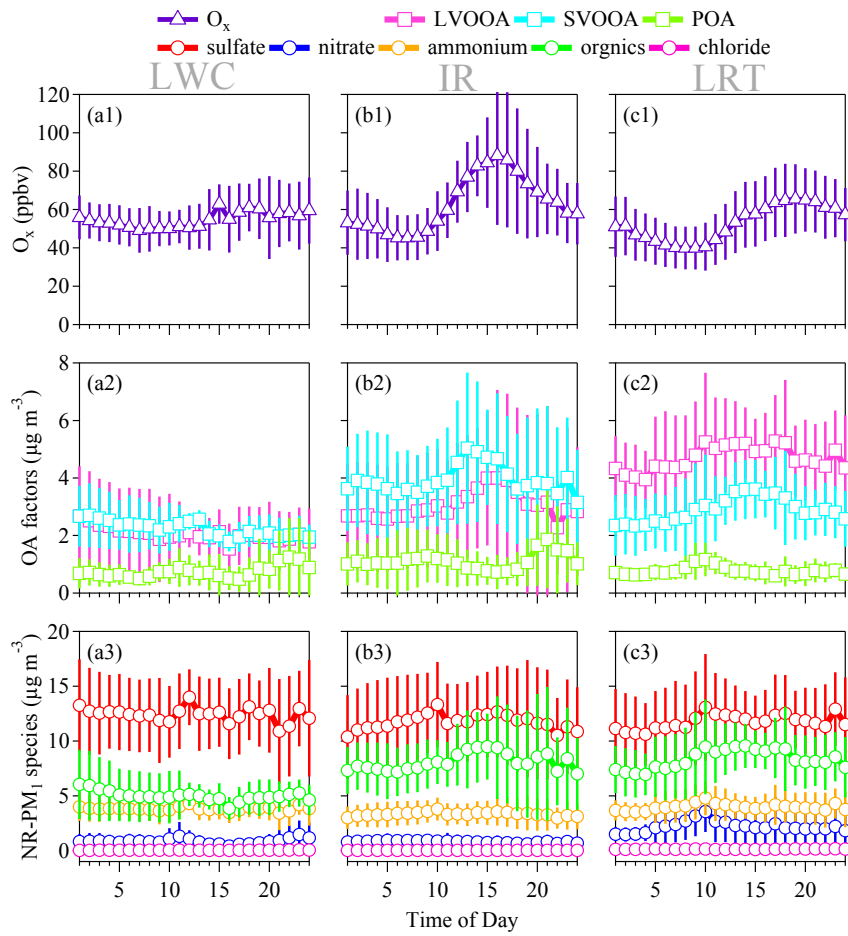
b: Direction of air mass origin: Northeast (NE); Northwest(NW); North (N).

1 **Figures:**



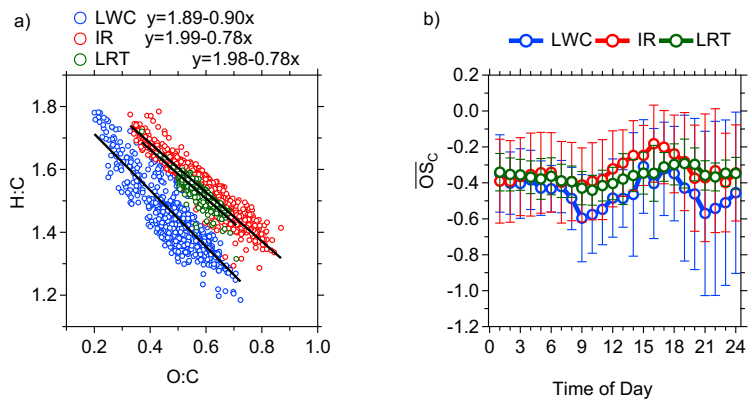
2

3 *Figure 1 Chemical constituents NR-PM₁ in LWC, IR and LRT episodes. (LWC: medium-range transport with high*
4 *LWC and low IR; IR: medium-range transport with high IR and low LWC; LRT: long-range transport)*



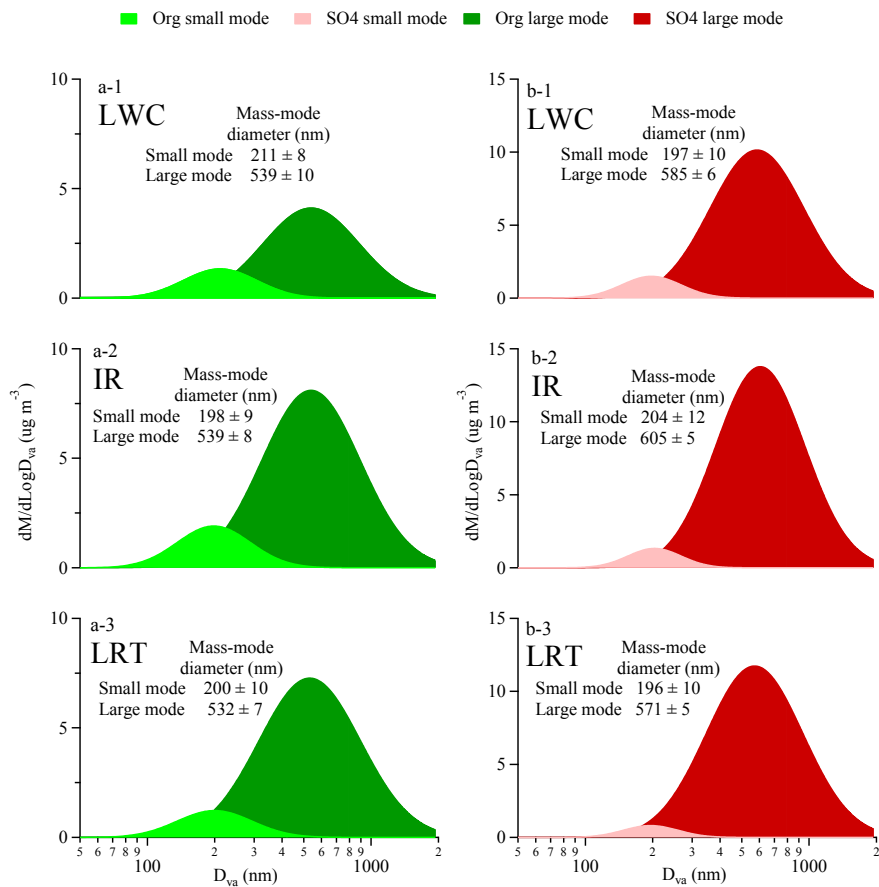
5

6 Figure 2 Summary of diurnal variations of the PM_{10} species, PMF-resolved organics as well as O_3 in the three types
 7 of episodes. Means are shown as points and standard deviations are as error bars.



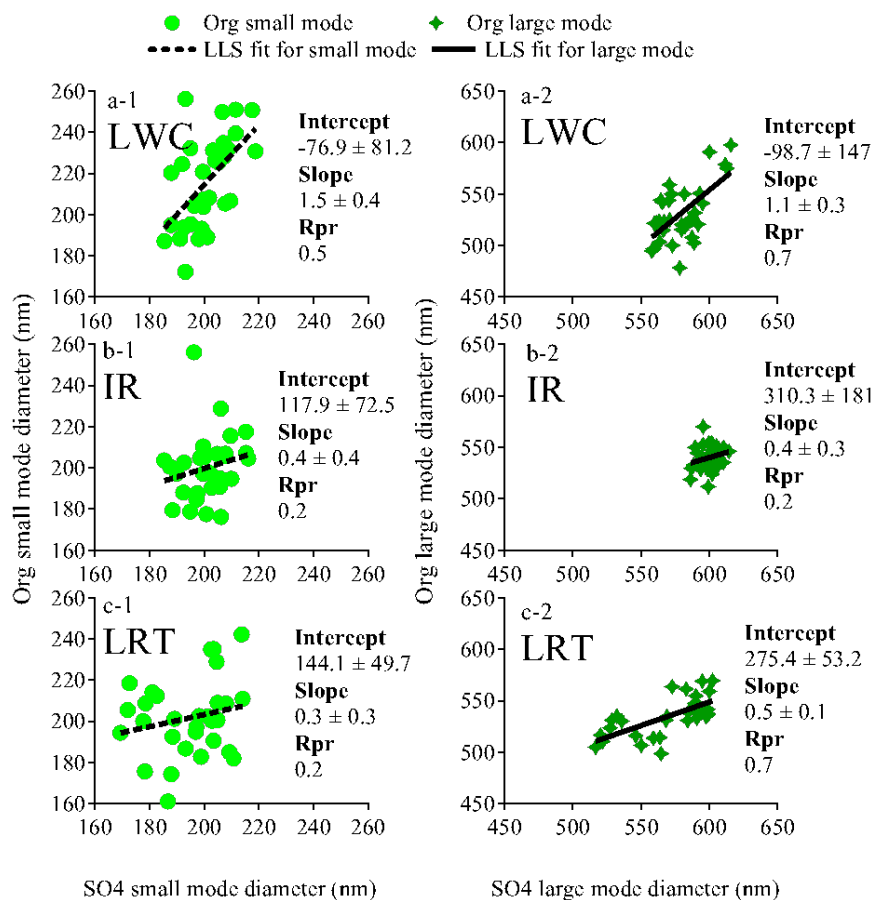
8

9 Figure 3 a) Van Krevelen diagram for the three types of episodes; b) diurnal variation of carbon oxidation state
 10 (OS_c). Means appear as circles with superimposed standard deviations.



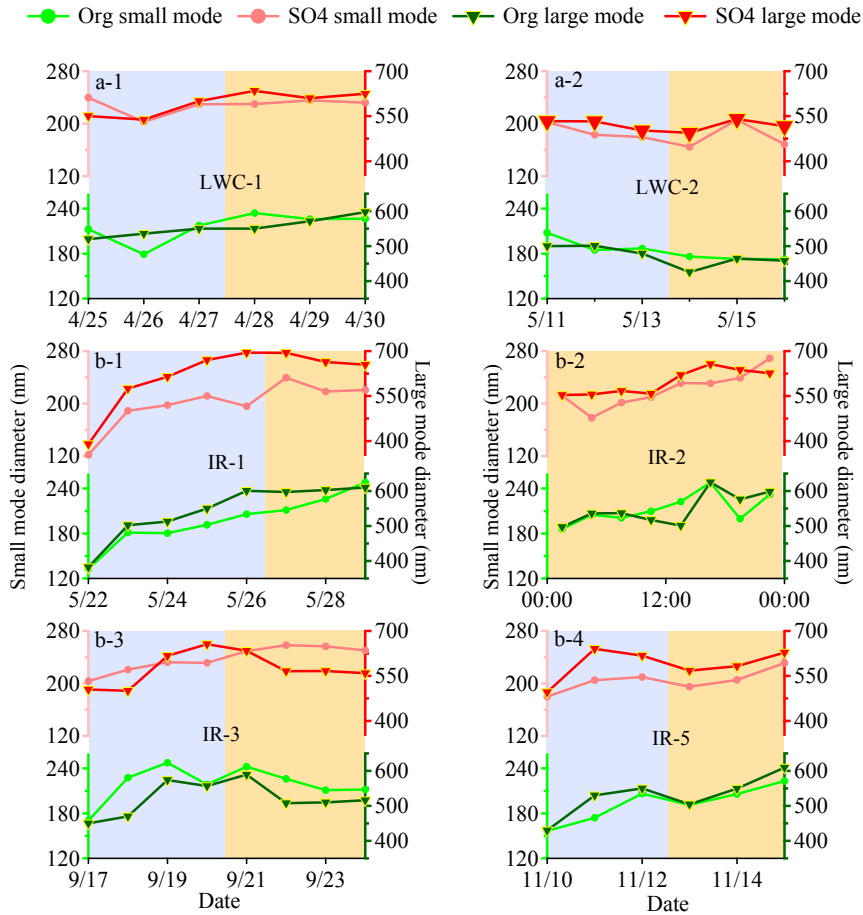
11

12 *Figure 4 Bimodal log-normal fitting results of the size distributions of organics and sulfate during the three types of*
 13 *episodes. a) Fitted small particle size mode and large particle size mode of organics during LWC, IR and LRT*
 14 *episodes; b) fitted small particle size mode and large particle size mode of sulfate during LWC, IR and LRT episodes.*



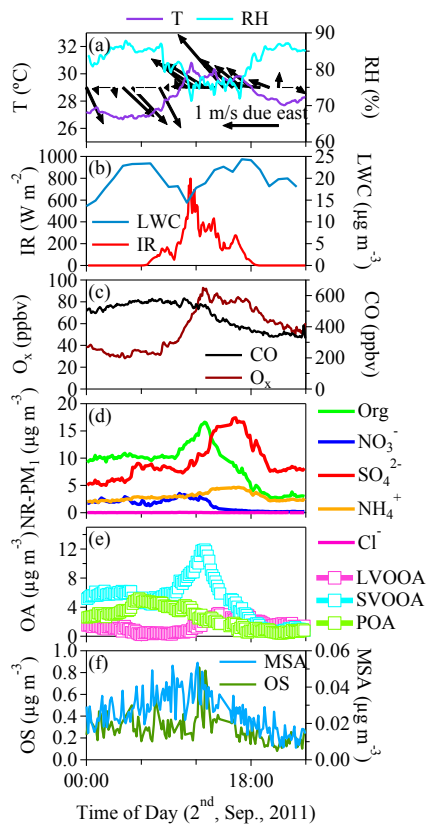
15

16 Figure 5 Scatter plots and linear least square fits of mass-mode diameters of organics and sulfate during the three
 17 different types of episodes. a1-a2) small and large mass-mode diameter of organics against sulfate during LWC
 18 episodes; b1-b2) small and large mass-mode diameter of organics against sulfate during IR episodes; c1-c2) small
 19 and large mass-mode diameter of organics against sulfate during LRT episodes.



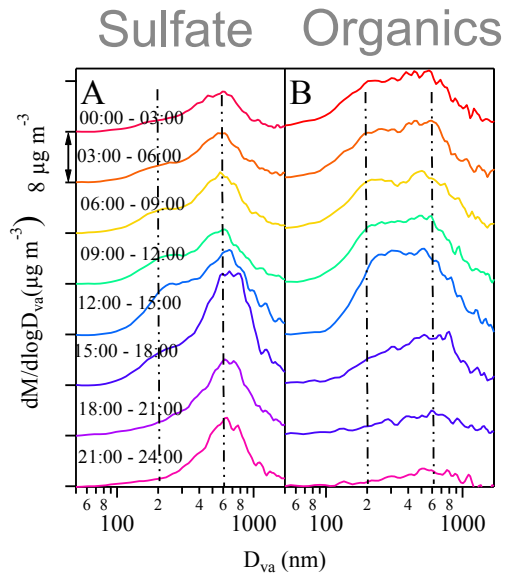
20

21 Figure 6 Variations of 24-hour averaged size distributions of fitted mass-mode diameters of organics and sulfates
 22 during LWC episodes and IR episodes (shaded in orange) and several days before each episode (shaded in blue).
 23 For the episode that lasted only for a day (E4), 3-hour averaged size distributions of fitted mass-mode diameters are
 24 shown instead. a) LWC episodes; b) IR episodes.



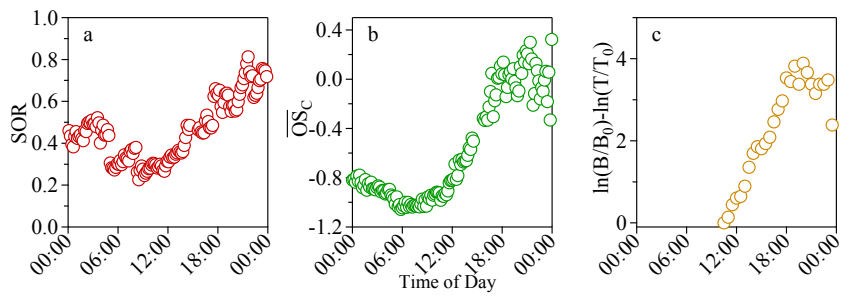
25

26 Figure 7 Time series of meteorological parameters, gaseous species, NR-PM1 species and PMF-resolved organic
 27 factors in E4.



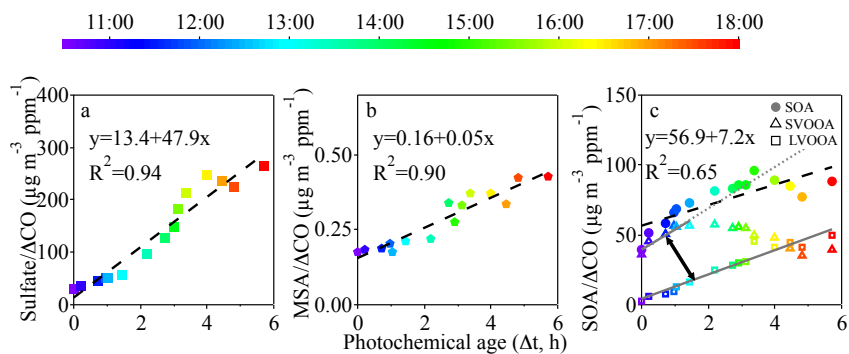
28

29 *Figure 8 Size distributions of sulfate (A) and organics (B) in different time intervals during E4.*



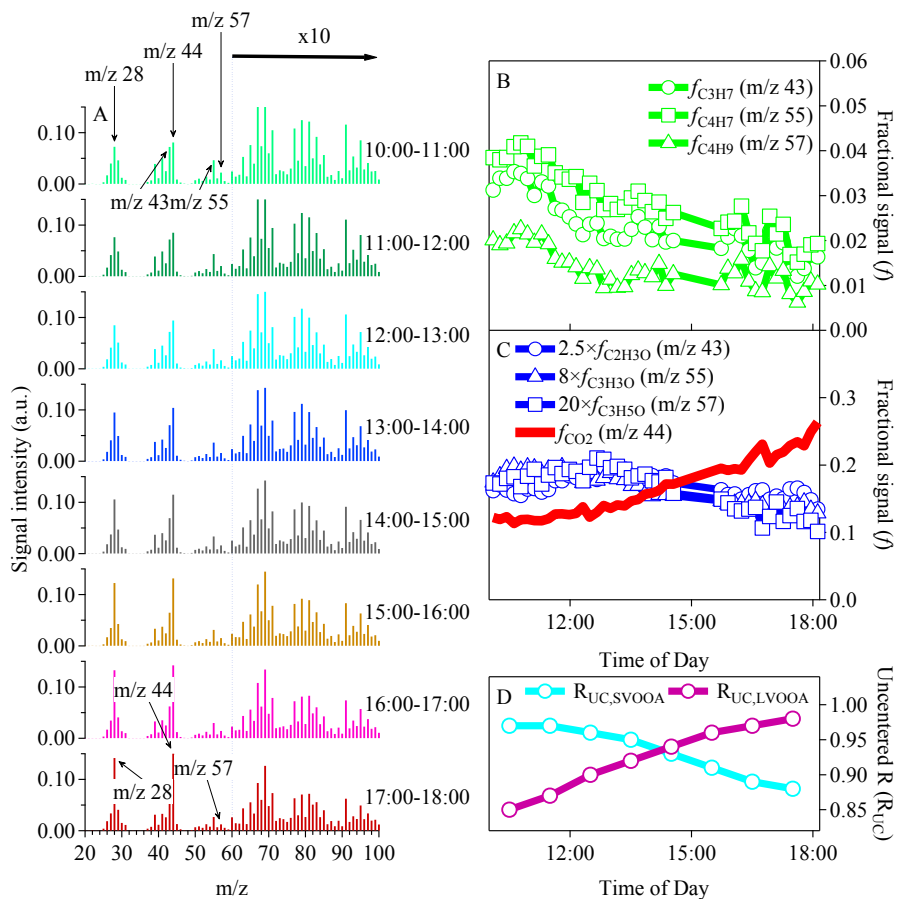
30

31 *Figure 9 Oxidative evolution of aerosol components. a) Sulfur oxidation ratio (SOR); b) average carbon oxidation*
 32 *state \overline{OS}_c ; c) benzene to toluene ratio (B: benzene concentration at time t; B0: benzene concentration at time 0; T:*
 33 *toluene concentration at time t; T0: toluene concentration at time 0).*



34

35 *Figure 10 Photochemical production of secondary species. a) Δ CO-normalized sulfate concentration ($SO_4/\Delta CO$)*
 36 *as a function of photochemical age; b) Δ CO-normalized MSA concentration ($MSA/\Delta CO$) as a function of*
 37 *photochemical age; and c) Δ CO-normalized secondary organic aerosol concentration ($SOA/\Delta CO$,*
 38 *$SOA(SVOOA+LVOOA)$) as a function of photochemical age. Data points are colored by time of day. Data points*
 39 *represent half-hour averages.*



40

41 *Figure 11 Evolution of high-resolution organic mass spectra from 10:00 to 18:00 during the photochemical aging*
 42 *process in E4: a) mass spectral evolution; b) changes in relative intensities of hydrocarbon-like ions $C_3H_7^+$ (m/z 43),*
 43 *$C_4H_7^+$ (m/z 55) and $C_4H_9^+$ (m/z 57); c) changes in relative intensities of oxygen-containing ions: $C_2H_3O^+$ (m/z 43),*
 44 *$C_3H_3O^+$ (m/z 55), $C_3H_5O^+$ (m/z 57) and CO_2^+ (m/z 44); and c) correlation of OA mass spectra with reference (Mohr et*
 45 *al., 2012) SVOOA and LVOOA mass spectra.*

Frequency of high PM1 episodes

As is apparent from Table 1, the occurrence of different types of episodes exhibits a seasonal trend. LWC episodes occurred only in spring and LRT episodes only in winter, while IR episodes took place in spring, summer and autumn. This result is consistent with previous results (Huang et al., 2009) in that the frequency of high PM days in Hong Kong had a strong seasonal variation. In winter, the overwhelming northerly wind brings pollutants via long-range transport (Fang et al., 1999). In spring, foggy days with high PM levels are common due to the moisture-laden air masses coming in from the sea and aqueous-phase processing of particulate species (Li et al., 2013). In summer, however, hazy days are mainly due to high photochemical activities in this subtropical area, resulting in the formation of secondary aerosols (Hu et al., 2008; Zhou et al., 2014).